CHIP-SCALE MAGNETIC SOURCE OF COLD ATOMS

THESIS

Eric A. Imhof, CTR

AFIT-ENP-13-J-03

DEPARTMENT OF THE AIR FORCE
AIR UNIVERSITY

AIR FORCE INSTITUTE OF TECHNOLOGY

Wright-Patterson Air Force Base, Ohio

AFIT-ENP-13-J-03

CHIP-SCALE MAGNETIC SOURCE OF COLD ATOMS

THESIS

Presented to the Faculty

Department of Engineering Physics

Graduate School of Engineering and Management

Air Force Institute of Technology

Air University

Air Education and Training Command

in Partial Fulfillment of the Requirements for the

Degree of Master of Science in Applied Physics

Eric A. Imhof, B.S. in Physics

CTR

June 2013

AFIT-ENP-13-J-03

CHIP-SCALE MAGNETIC SOURCE OF COLD ATOMS

Eric A. Imhof, B.S. in Physics
CTR

Approved:

Glen P. Perram, PhD (Chairman)	Date
Matthew B. Squires, PhD (Member)	Date
David E. Weeks, PhD (Member)	Date

AFIT-ENP-13-J-03

Abstract

Numerous disruptive technologies are being hampered by the insufficient modern methods of cooling electrically neutral atoms and molecules. Microchip-based magnetic deceleration provides a cooling mechanism to slow most neutral atoms and molecules within the cost and size requirements of a real-world device. Simulations of a novel deceleration technique show 90% removal of kinetic energy from an atomic beam. An experiment is built which creates a time-dependent, decelerating magnetic field to slow an atomic beam. An atomic beam is magnetically guided 800 microns above the surface of a microchip at pressures of 10^{-9} Torr. A 60 independent wire microchip is fabricated, controlling 200 A currents through 150 micron wide wires with a 90% success rate. Flaws are identified and future efforts to correct them are discussed.

To my new wife, my parents, and my brothers. I am not supposed to put names in the dedication, but no one said anything about memories. So remember a baseball to the chin the day before your first communion, racing a thunderstorm to shore after fishing on the barge, and 7 x 7 = 49 because mom asked you to help me learn multiplication tables. Then remember the fear of the diagnosis and the quiet joy when it was over. Remember waking up before the sunrise to help me find sand dollars on the beach. White roses, melting rotunda ice cream, cantering in the desert, the roof of the physics building, no air conditioning, shooting stars, coconut and coconuts, hacienda, and margarita.

Acknowledgments

I would like to thank Dr. Matt Squires for his extraordinary mentorship before and throughout my studies at AFIT. Working with him rekindled my desire to pursue this degree at a time when I was prepared to drop physics altogether (to pursue neuroscience, no less, the horror!). His support, friendship, and faith in my work has been a model which I hope to emulate, and I hope this thesis does that justice.

Thank you to the entire Cold Atom Group of the Air Force Research Laboratory for welcoming me and helping me with this research. The Cold Atom Group took the risk of funding this effort, and acted as my home laboratory. I would have been computationally lost without Dr. Spencer Olson, who also gave significant insight into the development of the theory described here. Thank you Dr. John Burke, Dr. Chris Erickson, Dr. Brian Kasch, Dr. Nate Zameroski, Lt. Evan Carlson, and Cpt. Brian Foo. Thanks especially to Lt. Jonathan Crow, whose machining and workshop skills were a crucial asset.

Thank you to Dr. Perram, my thesis advisor, for his willingness to take on a new subject, for guiding my studies, and for taking the financial burden of my studies here. Thanks Dr. Weeks for being on my committee. Thank you to AFIT and Dr. Giles, the head of the department, for a great two years. I am proud to be affiliated with this institution.

Eric A. Imhof

Table of Contents

Page

Page

List of Figures

List of Tables

List of Symbols (in approximate order of appearance)

Symbol	Definition
λ	Particle quantum wavelength (m)
h	Planck's constant (J s)
p	Particle momentum (kg m/s)
Λ	Ideal gas thermal quantum wavelength (m)
k_B	Boltzmann constant (m^2 kg/ s^2 K)
T	Temperature (K)
I	Current (A)
μ_0	Permeability of free space (N/A^2)
μ_B	Bohr magneton (J/T)
v_0	Initial speed of target atom (m/s)
ρ	Inverse of the time constant of the exponential slowing function (Hz)
t	Time (s)
α	Distance from beam to chip surface (m)
β	Half distance between wires (m)
$\zeta(t)$	Equation of motion of time-dependent magnetic field (m)
$\vec{B}$	Magnetic field (T)
V	Potential (J)

CHIP-SCALE MAGNETIC SOURCE OF COLD ATOMS

I. Background

1.1 Cold Atoms

1.1.1 The Basics.

The study of cold atoms is a subset of statistical physics, examining distributions of gaseous atoms in the sub-Kelvin temperature regime. When a confined gas of atoms is cooled past a certain threshold, quantum effects become apparent. On a broad level, this can be understood by the de Broglie wavelength, which states that the spatial extent of matter is inversely related to its momentum by

$$\lambda = \frac{h}{p} \tag{1.1}$$

where h is planck's constant, and p is the particle's momentum. This idea can be extended to the thermal de Broglie wavelength, which is the average spatial extent of a particle in an ideal gas, defined as

$$\Lambda = \frac{h}{\sqrt{2\pi m k_B T}} \tag{1.2}$$

where m is the mass of the particle, k_B is the Boltzmann constant, and T is the temperature.

Therefore, as a cloud of atoms falls in temperature, the average wavelength of the constituent atoms increases. At a threshold temperature and density, these matter waves begin to overlap, constructively interfering to form a macroscopic matter wave that can be observed and manipulated.

1.1.2 Current and Potential Uses.

Cold atoms have a number of uses mostly taking advantage of quantum matter-wave interference arising from the crossing of two cold atom clouds. These applications, like their optical interferometry predecessors, offer dramatic improvements in precision measurement. Applications include inertial navigation and gravitational gradient detection.

Cold atoms are used to define time. In an atomic clock, a beam of atoms passes through a cavity filled with microwaves. The microwave radiation will induce some of the atoms to transition into a higher energy state. The beam then exits the cavity and is probed by a laser which induces the atoms in the altered state to emit light. The emitted light is measured for a range of microwave frequencies in the cavity. When the intensity of the emitted light is a maximum, then the microwave frequency corresponds to the known transition frequency for the atom. By locking the microwave cavity to the transition frequency, an accurate, stable clock is produced. By cooling the atoms, the Doppler broadening of the beam diminishes, improving the certainty that the atom transitioned at the calculated frequency and improving the signal to noise ratio of the clock. Accurate clocks are integral to sensitive technologies such as the Global Positioning System.

Cold atoms could enable several new experiments. For example, in cold chemistry, chemical reactions that usually occur too quickly for direct measurement can be slowed and observed. Additionally, cold atoms are being considered as the foundational basis of a quantum computer, as they can be entangled to create a physical quantum bit. However, many of these technologies and experiments are either hindered or stopped altogether by the limited means of cold atom production.

1.1.3 Current Methods of Cold Atom Production.

1.1.3.1 The Magneto-Optic Trap.

The effective standard for creating cold neutral atoms is the magneto-optic trap (MOT) [2], [9]. In a MOT, a pure gas of neutral atoms is illuminated in three axes by intersecting,

retro-reflecting laser beams red-detuned from an atomic transition. If an atom in the gas approaches one of the lasers, it will experience a Doppler-shifted frequency and absorb a photon. The absorption gives a momentum kick to the atom in the direction of the laser's propagation. The atom will then re-emit the photon in a random direction, and have its momentum change correspondingly in the opposite direction. As this process is repeated, the absorption always pushes the atom in the beam direction, while the random re-emission, summed over many events, causes no net momentum change. The result is a velocity-dependent force in the beam direction.

Because the absorption/re-emission process must repeat many times for the atom to slow appreciably, MOT's require atoms with a closed optical loop. In a closed loop, the atom absorbs to a higher energy state and re-emits back to its original state so the process can repeat. If this closed loop does not exist, meaning the excited atom can transition into a different lower state, then extra lasers are required to "repump" the atom back to the cooling transition.

The Doppler-dependent force from the laser will slow the atom while it has velocity in the beam's direction, but it will not push the atom the opposite direction. Instead, a magnetic field is used to capture these slowed atoms in the same location. The magnetic field has a minimum at the beam intersection. As an atom travels to regions of higher magnetic field, each of its energy levels is split into multiple states with different energies. This "Zeeman shift" in energy levels will bring the atom into resonance with the detuned cooling laser, allowing it to absorb a photon. Thus, the cooling light now causes a force dependent on the position of the atom in the magnetic trap. This combination of both a velocity and position dependent restoring force provides a robust cooling mechanism capable of taking a room temperature gas to the sub-Kelvin regime.

The MOT can operate in three dimensions to create a cloud of cold atoms, or in two dimensions to create a cold atomic beam. For the two-dimensional MOT (2D-MOT), a gas

of atoms is contained in a vacuum chamber with a small ($\approx 10^{-8}$ m^2) exit hole from which a cold atom beam will emerge. Two retro-reflecting lasers and a magnetic trap cool the transverse directions. It is unlikely that a thermal atom has the exact velocity orientation to exit the chamber. However, atoms with velocity mainly in the transverse directions will be cooled. Those atoms with slow longitudinal velocity and cooled transverse velocities will congregate at the magnetic minimum, which can be aligned with the exit hole. Thus, while high velocities can, with low probability, emerge in the beam, most of the beam atoms are slow in the beam direction ($\approx$ 8 m/s) and cooled in the transverse directions ($<$ 1 m/s) [2].

In the 2D-MOT, a flat mirror with the exit hole drilled in its center can be used as one wall of the vacuum chamber. Then a third cooling laser, called a "push beam," can be used to slow the longitudinal velocity of the beam further. This setup in referred to as the enhanced 2D-MOT, or the 2D$^+$-MOT.

While robust, the optical loop requirement makes the MOT difficult to use for atoms and molecules with complex energy structures. Meanwhile, lasers must exist to induce the required transitions. These limitations tend to restrict the MOT to using the alkali atoms, with their single valence electron. While complex efforts have been made to expand to other parts of the periodic table, the MOT is not a viable cooling mechanism for most neutral atoms.

1.1.3.2 The Zeeman Slower.

The other main source of cold neutral atoms is the Zeeman Slower. The Zeeman Slower uses optical slowing like the MOT [6], implying the same restrictions on which atoms can be used. Imagine a neutral atomic beam propagates towards a laser beam. The laser operates at the absorption frequency of the atoms in the beam minus a Doppler shift corresponding to the beam velocity. As the atoms absorb photons from the laser, they slow. As they slow, they will experience a new Doppler shift and stop absorbing.

To allow the atoms to absorb along the length of the slower, a static, spatially-varying magnetic field is imposed along the beam's propagation. As the slowing atom sees a decreasing Doppler shift, the Zeeman shift from the magnetic field compensates, keeping the atom on resonance.

Due to the same restrictions the MOT experienced while optical cooling, the Zeeman Slower is not a robust, extendable slowing device for neutral atoms past the alkalis.

1.1.3.3 The Stark Decelerator.

The current method to slow ions and electrically polar molecules is the Stark Decelerator. When an atom enters a region of high electric field, its energy levels will split into multiple states of different energies. This "Stark shift" removes kinetic energy from the particle depending on the strength of the field. If energy is conserved in the system, the shift will allow the ion to slow in regions of high electric potential and return to its original speed once it leaves those regions.

In a Stark Decelerator, a pulse from an ion beam is sent between alternating electrodes, the first of which is turned on. The ions will slow as they encounter the increasing electric field from the first electrode. However, before it can return to its original speed, the first electrode is turned off and its adjacent electrode turned on. Now, instead of accelerating, the ion experiences another increasing electric field, and decelerates further.

With each consecutive electrode, the beam decelerates. Thus, the Stark Decelerator is dependent on the strength of each electric field and the length of the slowing region. Stark Decelerators can be meters in length. On the other hand, a Stark Decelerator was recently demonstrated above the surface of a microchip [5].

Being based on the electric field, the Stark Decelerator operates only on ions and polar molecules. However, it serves as an analogue to the magnetic decelerator described in this thesis. In principle, a Zeeman Decelerator would work as described above, using the magnetic field instead of the electric field. In practice, the Zeeman Decelerator has

been difficult to achieve, as the magnetic field is inherently weaker than the electric field. Thus, creating a large enough field to decelerate a neutral atom beam is a significant design challenge.

1.2 Magnetic Slowing

1.2.1 Definition.

Pure magnetic slowing is an alternative cooling mechanism that uses only magnetic fields to decelerate an atomic beam. Magnetic slowers are a source for atoms too difficult to cool by optical or electrical means. Optical techniques require a well-understood electronic structure for the atom species to be slowed, which restricts most efforts to the alkali metals. Meanwhile, electric based slowing requires a charged atom or polar molecule to interact with the electric field. By contrast, magnetic slowing can work on any atom or molecule with a magnetic dipole moment, meaning over half the periodic table and most molecules [1].

1.2.2 Usefulness.

Various experiments require a particular element to be cooled, while other experiments could be more precise with elements which currently cannot be slowed. For example, in a cold atom interferometry experiment, measurements are made of the final spatial density of the atom clouds. The interferometry signal arises from the quantum matter waves interacting, so classical collisions create noise. Experiments could be made more precise by cooling new atomic species with minimal collisional cross-sections.

Magnetic slowing is conducive to miniaturization. Prior experiments have shown the creation of a Bose-Einstein Condensate on the surface of a microchip [3]. Using small etched wires on the chip to create magnetic trapping fields, these experiments first had to use a MOT to cool atoms from room temperature, requiring added space. A magnetic slowing source could be chip based as well, enabling the entire cold atom production, manipulation, and use to take place in a compact, cheaply produced area. Meanwhile,

replacing the MOT would reduce the number of lasers needed for the experiment, significantly reducing both size, cost, and complexity.

Magnetic slowing could enable the continuous matter wave laser [4]. At present, atom lasers are pulsed systems, as the cold atoms are created in a MOT, the lasers turned off, evaporative cooling performed, and the process repeated. With no need for lasers, magnetic slowing provides a source of cold, non-condensed atoms in close proximity to the condensate. Recent experiments in condensate distillation suggest a seed condensate surrounded by a replenishing source of cold thermal atoms may create a self-sustaining condensate.

Despite these benefits, magnetic slowing is still in the early stages of its development. Current methods, while valuable as proof of concept, are not feasible for use outside of the laboratory environment. Specifically, modern methods are not optimized for slowing length and dissipate large and unnecessary amounts of power.

1.2.3 Current Methods of Magnetic Slowing.

1.2.3.1 Time of Flight Slowing.

Prior efforts have been made at magnetic slowing. The simplest design works analogous to the Stark Decelerator. Imagine a pulse from an atomic beam is travels along the same axis as a series of solenoids, the first of which is turned on [7]. When the pulse reaches this first solenoid, it encounters a region of high magnetic potential, experiences an increasing Zeeman shift in its energy levels, and slows. Before the pulse exits the solenoid, the solenoid is turned off, and the next solenoid is turned on. As the atom pulse reaches the second solenoid, it slows further, and the process repeats.

The timing of when to turn on/off each solenoid is determined by what is called a "time-of-flight" (TOF) calculation. TOF means that an average or "synchronous" atom in the pulse is imagined and its trajectory mapped as it transits the series of solenoids. The solenoids are then turned on or off to match when this atom has arrived at each stage [8].

TOF decelerators are not optimized slowing systems. At each stage, a specific amount of energy is removed, then after some propagation time to the next stage, another specific amount of energy is removed. This piecewise defined slowing can be improved to shorten the slowing length of the decelerator and use energy more efficiently.

1.2.3.2 Continuous Motion Slowing.

Instead of a series of stages, a continuously varying magnetic potential moving with a precisely defined equation of motion could be more efficient than piecewise TOF slowing. This thesis proposes a unique equation of motion for a continuously moving magnetic potential which improves slowing distance.

Prior experiments have created a moving magnetic trap to perform continuous motion slowing [12]. The device was free space and macroscopic, not the chip based system made for this thesis. Additionally, their equation of motion for the magnetic trap was not optimized for a minimal slowing length.

II. Introduction

2.1 Chip-Scale Magnetic Slowing

Chip-Scale Magnetic Slowing is the attempt to decelerate a pulse of atoms from an atomic beam using magnetic fields produced by wires on a microchip fabricated using standard lithography and chip etching techniques.

2.1.1 Benefits.

The power dissipation of current (i.e. not chip-based) methods of magnetic slowing confines modern experiments to the laboratory. The magnetic field is inherently weak, requiring large currents to create a large enough potential energy to slow atoms. Because, the magnetic field is inversely proportional to distance from a current carrying wire, atoms will feel a stronger field the closer they are to the wire. For a macroscopic solenoid, this distance is on the order of a centimeter, while on a microchip, the distance to the slowing wire is on the order of a millimeter or less. However, because power is given by $P = I^2R$, where I is the current and R is the resistance of the wire, a tenfold increase in distance requires a hundredfold increase in dissipated power to achieve the same strength field.

Meanwhile, a chip-based magnetic slower has minimal required size. Even the proof-of-concept chip to be described here will be a mere square inch in total area. Similarly, as all the necessary components are standard electronics pieces and all fabrication techniques are fairly straightforward, the cost of production is minimal.

2.1.2 Difficulties.

There are numerous difficulties impeding the creation of a chip-scale magnetic slower. First, for a chip to make a strong enough magnetic field to effect an atomic beam, the beam must pass extremely close to the chip surface. In this thesis, the atom beam will travel a mere 800 microns above the chip surface. Therefore, confinement and guiding of the beam is a significant challenge.

Even with the beam so close to the chip surface, creating large enough magnetic fields requires higher currents passing through smaller wires than most chips can handle without failure. Heat management will be a constant issue.

As the atom beam passes, miniaturization of the device implies that the slowing magnetic field move at comparable speeds to the beam. To do that, precision control of the high currents must be achieved, as well as precision timing. In the chip to be described, we will switch a 200 A current between adjacent wires in 20 μs.

2.2 Outline of Our Design

Our device will be a continuous motion slower with a unique slowing equation of motion to provide efficient deceleration in a small distance. Defining characteristics include the base chip material, the independently controlled slowing wires, the confining magnets, and the optimized equation of motion to slow the beam.

2.2.1 Base Chip.

To address the thermal difficulties of running high currents through microchip scale wires, we need a base chip with excellent thermal conductivity. We use direct-bonded copper (DBC) on an aluminum nitride (AlN) ceramic substrate [10]. In the DBC process, at a specific temperature and copper to oxygen ratio, a thin copper-oxygen layer forms between the copper and ceramic layers. This eutectic layer makes a chemical bond to both the copper and ceramic, facilitating an efficient heat transfer between them.

The DBC process works for several ceramics, notably beryllium oxide (BeO), aluminum nitride (AlN), and alumina (Al_2O_3). The DBC/BeO chip has the highest thermal conductivity, 260 W/m^{O}C. Unfortunately, BeO is a toxic material, and thus not conducive to the extensive troubleshooting and testing we need to perform. The DBC/Al_2O_3 has the least impressive thermal conductivity, at 25 W/m^{O}C. However, its low cost and bond strength have made it popular for power electronics applications. DBC/AlN offers a high thermal conductivity at 170 W/m^{O}C without the toxicity of BeO.

DBC/AlN chips offer other unique benefits. The DBC technique allows for significant copper layer depth, ranging from 25 to 300 microns. The DBC bond offers strong surface adhesion of the copper to the ceramic, allowing relatively rough handling during the fabrication process.

However, the DBC/AlN chips, being a thin ceramic, are prone to cracking. In our experiments, we found that any structural deficiency, even a thinning of the ceramic due to prolonged laser etching, significantly reduced the thermal capabilities of the chip. High-current wires would consistently fail in locations of highest stress or fracture.

Significantly, DBC/AlN microchips can be fabricated using well understood laser etching and lithography techniques. This allows rapid prototyping as well as precision production. Our 5.37 x 72.36 mm modular chips created for this experiment could be etched and ready in four to five hours. Our design was etched into the DBC using a laser etching machine capable of creating 100 micron features.

2.2.2 Independently Controlled Slowing Wires.

The chip-based slower will consist of a series of parallel, equally spaced, independent wires etched onto the chip. These wires will run perpendicular to the beam direction. Rather than use a vast array of power supplies, each wire will be controlled using a high-power transistor. Then, the wire will only draw current when its transistor is on.

When turned on, the wire creates a circular magnetic field which is inversely proportional to the radial distance, r, from the wire

$$\vec{B} = \frac{\mu_0 I}{2\pi r}\hat{\phi} \tag{2.1}$$

where I is the current and $\hat{\phi} = -\sin\phi\ \hat{i} + \cos\phi\ \hat{j} = \frac{-y}{\sqrt{x^2+y^2}}\hat{i} + \frac{x}{\sqrt{x^2+y^2}}\hat{j}$. Then, substituting $r = \sqrt{x^2+y^2}$,

$$\vec{B} = \frac{\mu_0 I}{2\pi}\left(\frac{-y}{x^2+y^2}\hat{i} + \frac{x}{x^2+y^2}\hat{j}\right) \tag{2.2}$$

By using a strong, static confining field in the directions transverse to the beam's motion, the transverse magnetic field component from the wire can be assumed to be negligible. The component of the field opposing the beam's motion will be used to slow the pulse of atoms.

2.2.3 Lorentzian Transfer/Continuous Hill Motion.

Assume the beam propagates at a constant height above the chip surface. At that height, the slowing (antiparallel to the beam) component of the created magnetic field forms a Lorentzian peak centered at the wire's position. We wish to make this magnetic field move continuously according to some function $\zeta(t)$. We will derive our choice for $\zeta(t)$ in later sections. For now, consider it as an arbitrary function. We will vary the currents in adjacent wires to transfer the Lorentzian magnetic potential as a function of time from one wire to the next, as shown in Fig. 2.1. Thus we can move continuously between a series of wires with a maximum of two independent currents flowing at any given time.

Suppose the beam propagates along the z-axis of a right hand coordinate system, and the slowing wires run along the y-axis. Let the wire separation be 2β. Then, when a single wire turns on, its magnetic field in the $\hat{k}$ direction at $(x, y, z) = (0, 0, z)$ will be

$$\vec{B}_z = \frac{\mu_0 I_n}{2\pi}\left(\frac{\alpha}{\alpha^2 + (z - 2n\beta)^2}\right)\hat{k} \tag{2.3}$$

where α is the constant height above the slowing chip, and I_n is the current for the n^{th} wire, assuming the first wire is located at $z = 0$. Then, if our magnetic potential is to move according to the function $\zeta(t)$ between wire $n-1$ and n, we will try to add the two stationary but time-dependent Lorentzians to create a single moving one. Explicitly,

$$\frac{\mu_0 I}{2\pi}\left(\frac{\alpha}{\alpha^2 + (z - 2(n-1)\beta + \zeta(t))^2}\right) = \frac{\mu_0 I_{n-1}(t)}{2\pi}\left(\frac{\alpha}{\alpha^2 + (z - 2(n-1)\beta)^2}\right) + \frac{\mu_0 I_n(t)}{2\pi}\left(\frac{\alpha}{\alpha^2 + (z - 2n\beta)^2}\right) \tag{2.4}$$

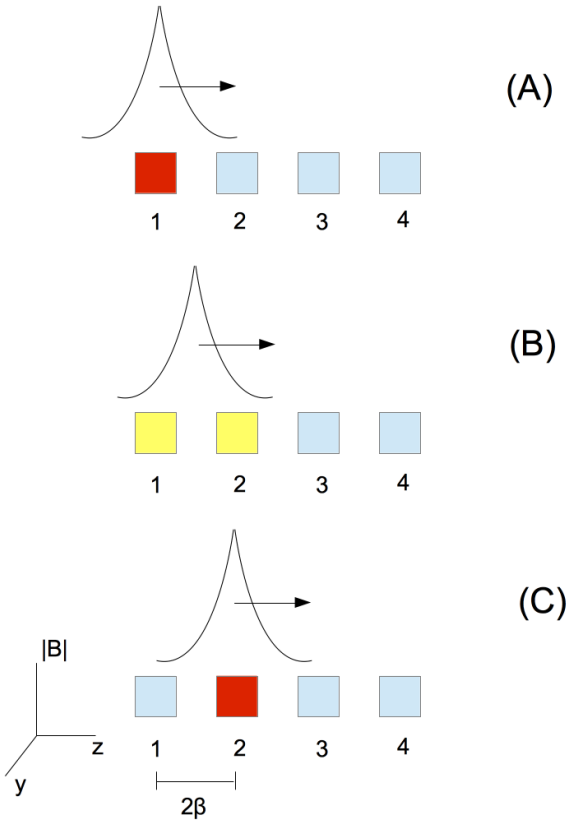

Figure 2.1: Magnetic potential transferring between adjacent wires. In (A), wire 1 is fully on, carrying the maximum current. In (B), wires 1 and 2 are partially on to move the potential between 1 and 2. In (C), wire 2 is entirely on, and the process continues, moving the magnetic potential in a continuous fashion.

We take I on the left hand side to be constant, and attempt to vary I_{n-1} and I_n as functions of time to make the equation valid. Unfortunately, an exact solution cannot be found. However, under the conditions that $\beta << \alpha$, and that $\zeta(t)$, which ranges from 0 to 2β, is also $<< \alpha$, we find the condition

$$z - 2(n-1)\beta + \zeta(t) = \frac{I_{n-1}}{I}(z - 2(n-1)\beta) + \frac{I_n}{I}(z - 2n\beta) \tag{2.5}$$

$$\rightarrow I_n = I\frac{\zeta(t)}{2\beta} \tag{2.6}$$

and $I_{n-1} = I - I_n$.

2.2.4 Confining fields.

The confining fields act as the atom beam guide through the slowing region. They must form a consistent quadrupole field to restrict the beam's movement in the transverse direction. Because we use this transverse confining field, we will be able to use a one dimensional model of the slowing process in the following section.

To create the confining field, the chip will use two permanent NdFeO magnets, magnetized normal to the plane of the chip. Placed on either side of the beam, and magnetized in opposing directions, they form a quadrupole field, with a zero directly between them, as shown in Fig. 2.2

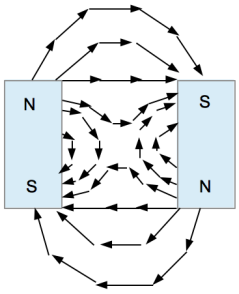

Figure 2.2: The field due to opposing permanent magnets.

In light of the approximations we made to transfer the Lorentzian potential between wires, we note that the spacing between slowing wires 2β should be $<< \alpha$, the distance from the chip surface to the atom beam. Because we made our wires as small as possible, $2\beta = 330$ microns. We thus chose $\alpha = 800$ microns, so that the permanent confining magnets can be a standard 1/16 of an inch thick.

2.3 Method of Slowing-Exponential Deceleration

A magnetic dipole moment $\vec{\mu}$ in an external magnetic field $\vec{B}$ experiences a potential energy $V = -\vec{\mu} \cdot \vec{B}$. The atom's electron spin creates a magnetic moment with a component aligned or anti-aligned to the external magnetic field. The component takes quantized values defined by the m_F states, which can take integer or half integer values. Then the potential energy felt by an atom in our beam is

$$V = m_F g_F \mu_B |\vec{B}| \tag{2.7}$$

where g_F is the Lande g-factor, and μ_B is the Bohr magneton. Idealizing the setup described above as a one dimensional system (see the Appendix for full 3D treatment), the atom will experience the moving potential

$$V = \frac{m_F g_F \mu_0 \mu_B I_n}{2\pi} \left[\frac{\alpha}{\alpha^2 + (z - \zeta(t))^2} \right] \tag{2.8}$$

Then, because $F = m\ddot{z} = -\nabla V$ evaluated at $z = z_p(t)$, the position of the atom,

$$\ddot{z}_p = -\gamma \frac{z_p - \zeta}{[\alpha^2 + (z_p - \zeta)^2]^2} \tag{2.9}$$

where $\gamma = \frac{\alpha |m_F g_F| \mu_0 \mu_B I_n}{m\pi}$. Note that t has been suppressed from $z_p(t)$ and $\zeta(t)$ for aesthetic purposes. Let us assume that the solution takes the form

$$\zeta(z_p) = z_p + f(z_p) \tag{2.10}$$

where $f(z_p)$ is some correction factor. As such,

$$\ddot{z}_p = -\gamma \frac{f}{[\alpha^2 + f^2]^2} \tag{2.11}$$

which can be rewritten as

$$f^4 + 2\alpha^2 f^2 + \frac{1}{C} f + \alpha^4 = 0 \tag{2.12}$$

where $C = \ddot{z}_p/\gamma$. The equation is quartic, and yields complete, closed, analytic solutions for $f(z_p)$ in terms of C. Thus, if $\ddot{z}_p$ can be written as a function of t, then we have solved for the necessary time dependent potential to make the atom move according to the trajectory $z_p(t)$.

Notice the importance of that statement. By being able to move the atom according to *any* trajectory, we can choose trajectories with short slowing distances. In other words, we can slow an atomic beam in the minimal slowing length provided by a microchip.

For example, consider what $\zeta(t)$ will force an ideal atom at speed v_0 and initial position $-v_0/\rho$ to experience an exponential decay in velocity. If successful, the atom will move according to the equation of motion $\ddot{z}_p = \rho^2 z_p$. As a function of time, $\ddot{z}_p = -v_0\rho \exp(-\rho t)$. Therefore, the potential is should be moved according to

$$\zeta(t) = -\frac{v_0}{\rho} e^{-\rho t} + f(t) \tag{2.13}$$

where $f(t)$ is found by substituting $\ddot{z}_p = -v_0\rho \exp(-\rho t)$ into Eq. 2.12. As $f(t)$ is the solution to a quartic, its analytic expressions are long and do not yield intuitive results. However, we can tell from the plots in Fig. 2.3 that $f(t)$ is only a small correction factor in $\zeta(t)$. Thus, we can approximate $\zeta(t)$ as just the exponential slowing term.

By using the exponential decay, the atom's velocity will approach zero as time approaches infinity. However, the required slowing distance is a mere $d = v_0/\rho$. We can adjust ρ as necessary to give as short a slowing length as needed.

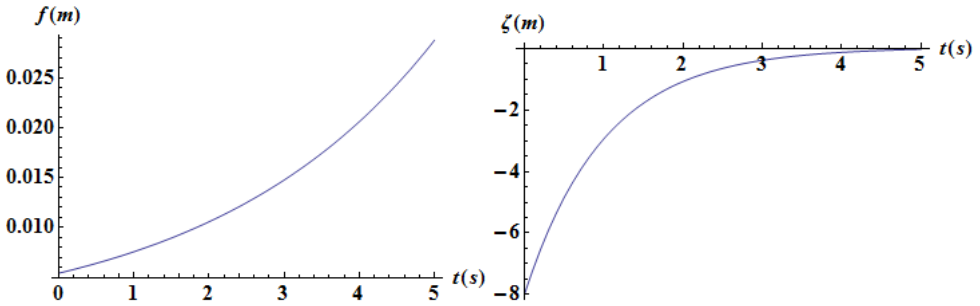

Figure 2.3: The exponential correction factor $f(z_p)$ and the full $\zeta(t)$ as a function of time, found by setting $v_0 = 8$ and $\rho = 1$.

Using 5^{th}-order Runge-Kutta methods, we simulated a pulse of atoms interacting with such a moving potential by integrating Equation 2.9. We simulate a two-dimensional magneto-optic trap beam ($2D^+$-MOT) interacting with a Lorentzian potential moving in one dimension according to $\zeta(t)$. For simplicity, $\rho = 1$. While this implies an unattainably long slowing length, it is useful to see that our simulations produce expected results.

The $2D^+$-MOT has a peak velocity of $v_0 = 8$ m/s. The longitudinal velocity distribution is approximately gaussian, with a FWHM of 3.3 m/s. The FWHM $\approx 2.3548\sigma_v$, so $\sigma_v \approx 1.4$ m/s. This corresponds to a temperature of 20.5495 mK (using $\sigma^2 = kT/m$). It creates a peak flux of 9 X 10^9 atoms/s [2]. We simulate a pulse duration of 1 ms. Our results are shown in Fig. 2.4.

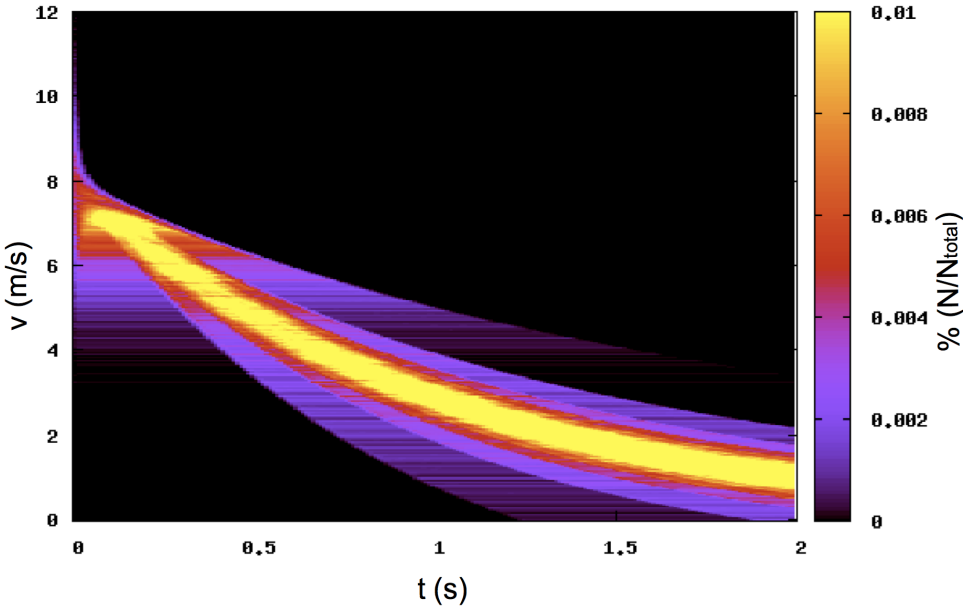

Figure 2.4: The exponential slowing of an 8 m/s atomic beam with the velocity distribution plotted as a function of time. The percent of the total beam pulse is plotted in the z-axis as a color scheme. Here, ρ = 1 Hz.

We explored the feasibility of slowing higher velocities over even shorter time intervals by modeling a higher peak velocity of 30 m/s with ρ increased to 1000 s^{-1}. The beam was slowed over a distance of 3 cm. Our results are shown in Fig. 2.5.

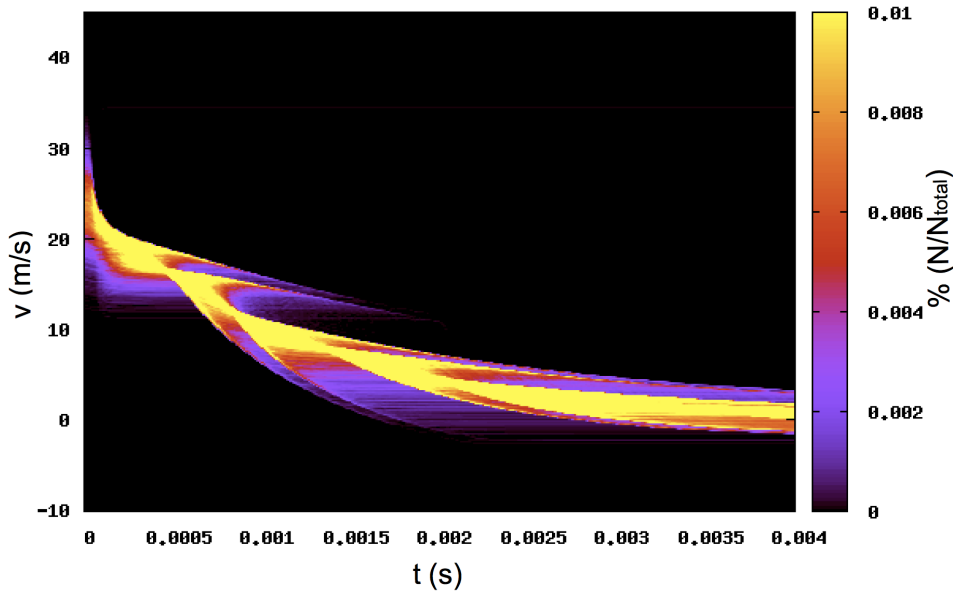

Figure 2.5: The exponential slowing of a 30 m/s atomic beam with the velocity distribution plotted as a function of time. The percent of the total beam pulse is plotted in the z-axis as a color scheme. Here, ρ = 1000 Hz, corresponding to a 3 cm long slowing region.

Both plots show the basic expected exponential slowing, but there are unexpected features in each plot. To get a better understanding of what creates these features, a three dimensional model was built of the 8 m/s beam, this time slowed across a 3 cm chip. The trajectories of a few selected initial velocities were plotted in the $\hat{i}$, $\hat{j}$, and $\hat{k}$ directions, shown in Fig. 2.6.

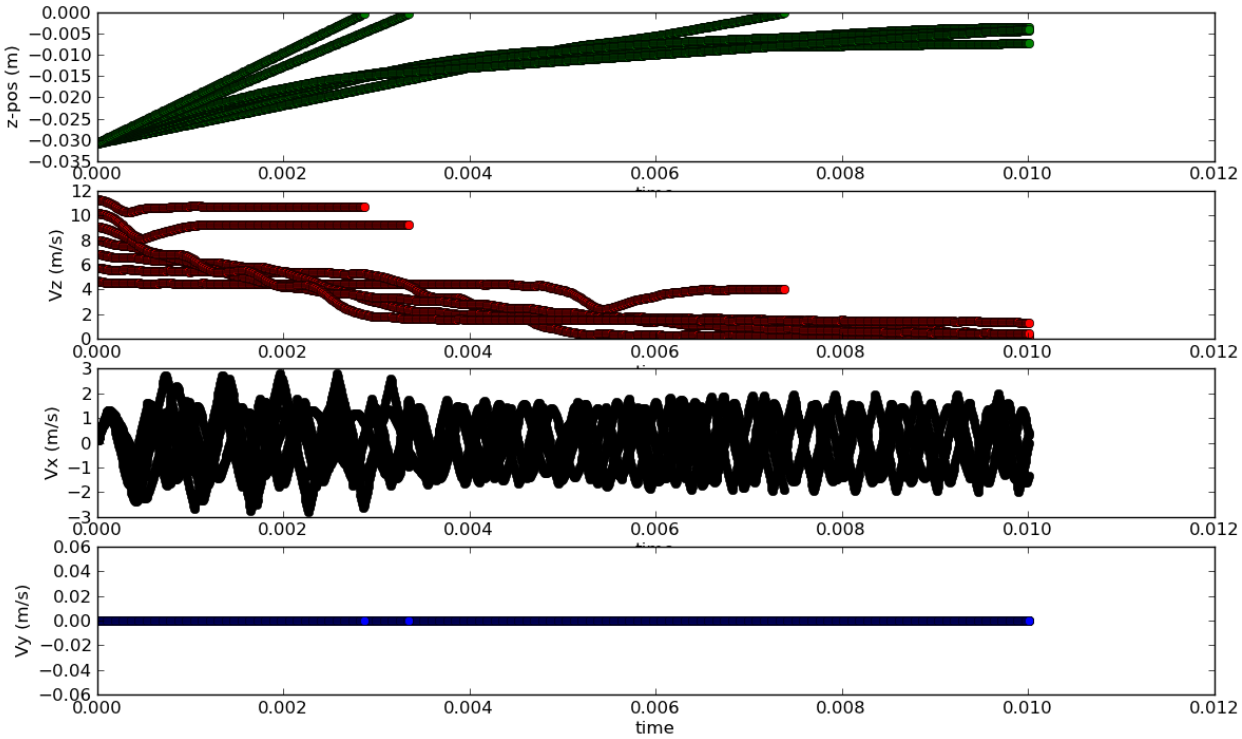

Figure 2.6: The exponential slowing of an atomic beam with the velocity distribution plotted as a function of time.

Here, the longitudinal velocity, v_z, is shown in red. The program ceases to plot the atom's trajectory after it leaves the slowing region, and it becomes clear that the non-exponential features in the previous plots represent atoms which have climbed over the slowing potential, accelerated afterwards, and exited the slowing region. In other words, the shorter $\rho = 1000$ Hz slowing chip lost more atoms than the long $\rho = 1$ Hz slowing chip. The faster moving potential had less tolerance for atoms not moving at the exactly correct initial velocity.

Further, the 3D model shows the validity of our assumption that the confining magnets kept the beam traveling at a relatively constant height above the chip surface.

The assumption was based on the significant relative strength of the confining magnets compared with the field from the slowing wires. However, the $\hat{i}$ component of the slowing field from the wires does exist, and it gives an initial kick to the atoms in that direction. That kick sets up a transverse oscillation seen in the v_x plot in Fig. 2.6.

The simulations show that a pulse of atoms from an atomic beam can be slowed to nearly zero velocity over microchip scale distances (3 cm). If an experiment could prove the simulations correct, it would represent a significant step towards taking magnetic slowing out of the laboratory and into new technologies enabled by cold atoms.

III. Detailed Design and Fabrication

3.1 Outline of the Overall Experiment

Cold atom experiments must take place under ultra-high vacuum (UHV) conditions. The cold atoms must be thermally isolated from the outside world, and a less than perfect vacuum provides an undesirable thermal link. Therefore, the built system uses a series of UHV chambers. These chambers are constructed using glass (Pyrex), DBC/AlN chips, NdFeO magnets, stainless steel, and copper gaskets, held together with bolts and epoxy. The epoxy is EpoTek 353 ND, which passes NASA's low outgassing standard ASTM E595 once properly cured [11].

The experiment uses a two dimensional enhanced MOT ($2D^+$-MOT) as a source beam. The $2D^+$-MOT will require two perpendicular, equal power, opposite circular polarization laser beams which intersect in a UHV chamber populated with ^{87}Rb. These lasers cool the gas in two of the three cardinal directions. The third direction is left free for the beam to propagate. Four magnets, external to the system, will create a minimum in the magnetic field where cold ^{87}Rb atoms populate to form the atomic beam.

The atomic beam provides a flux of 9 X 10^9 ^{87}Rb atoms/s, a peak velocity of 8 m/s with a FWHM of 3.3 m/s, and a beam divergence of 43 mrad [2]. The $2D^+$-MOT's slow and narrow velocity range, high intensity, and small divergence serve as an excellent source beam for a proof of concept.

The minimal velocity allows significant slowing to occur using weaker and therefore more easily controlled currents. Meanwhile, the high intensity and low divergence provide a high degree of predictability and measurability. Additionally, the $2D^+$-MOT can be pulsed easily by simply pulsing the lasers used to create it.

The beam pulse will leave the $2D^+$-MOT chamber and enter a narrow chamber characterized by the confining quadrupole magnetic field in the directions transverse to

the beam. One side of this chamber is the DBC/AlN chip. This chip will carry 60 equally spaced, independently controlled, parallel wires which run transverse to the beam direction. These wires will perform the slowing process.

The slowing chip will be controlled by a separate motherboard of 60 N-channel IRLB3813PbF International Rectifier MOSFET transistors. These transistors will be turned on and off by digitally controlling their gates using a Digital Input/Output System, the Viewpoint Systems DIO-64. When turned on, the transistors will pass 200 A up to individual wires on the slowing chamber chip.

Once the atoms have been slowed, they will enter an observation chamber, a simple six-sided rectangular glass structure which connects directly to an ion pump. The output from the slowing region will be observed by a laser approaching from the transverse direction, passing through the output atoms, and hitting a photodiode. A reference beam of equal power hits a separate photodiode. The two photodiodes will output currents which are proportional to the power of the beams which hit them. These two currents are combined into a difference circuit, so a difference in power caused by atoms in the observation chamber can be seen.

3.2 Making the Slowing Chip

3.2.1 AutoCAD design.

The slowing chip was designed using AutoCAD. It is made of five identical combined chips. Each chip has 12 independent wires. Six individual leads on the left join to a common bus on the right, while six additional independent leads on the right join to a common bus on the left. In the center, there is a 20 mm wide slowing region of independent, equally spaced wires. Each chip is 5.37 mm wide by 72.36 mm long. Each wire is 150 microns thick separated by 180 microns. The design is shown in Fig. 3.2.

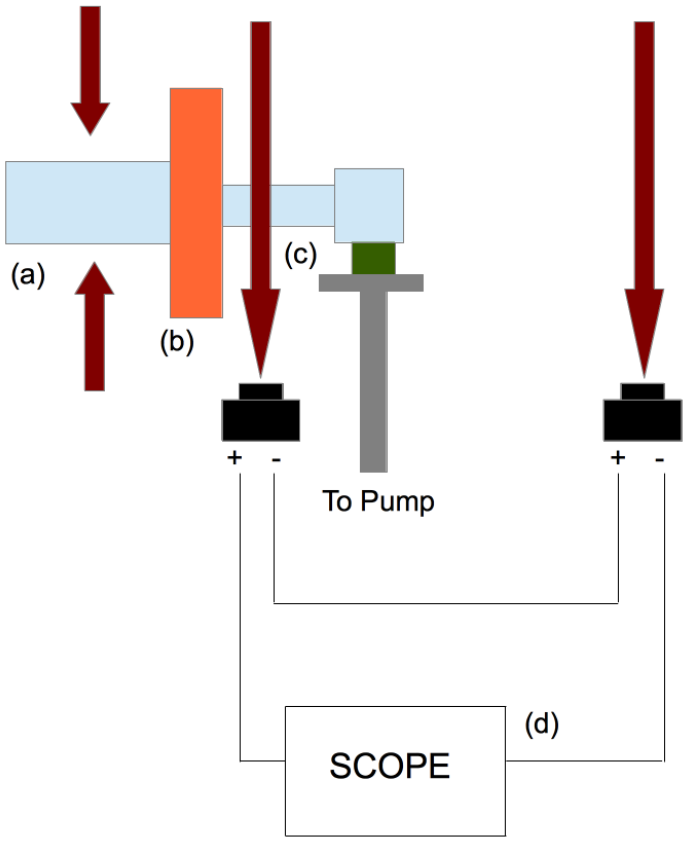

Figure 3.1: A sketch of the overall experiment. The $2D^{+}$-MOT chamber (a) and its associated cooling lasers, the slowing chamber (b), and the observation chamber (c), with its associated probe laser beams, photodiodes, and difference circuit (d).

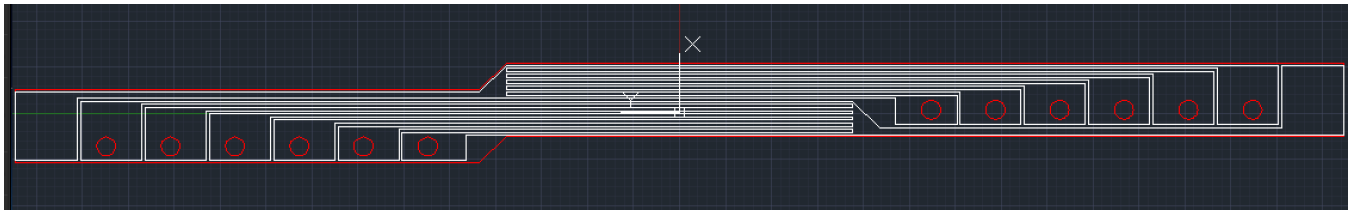

Figure 3.2: The modular slowing chip design. The chip is 5.37 mm wide by 72.36 mm long, carrying 12 wires, each 150 microns thick separated by 180 microns. The slowing region where all the wires overlap is 20 mm long.

Our prior designs placed all leads on one side of the slowing region, allowing them to connect to a common bus afterwards. However, each lead must be significantly wider than the 150 μm wire to which it connects. Therefore, the leads took up a large chip area, while the corresponding wires were forced to travel for long distances around them.

The prior designs were large ($\approx$ 160 cm^2). At this scale, the excellent thermal conductivity of the DBC/AlN worked against us, dissipating heat too quickly and making hand soldering nearly impossible. Further, large designs, like that shown in Fig. 3.3, were all-in-one, meaning every wire was on the same chip. If the chip was dropped, cracked, or broken for some reason, the entire fabrication process would have to be redone. Laser etching the chip in Fig. 3.3 took a full week. Clearly, a modular design would be beneficial.

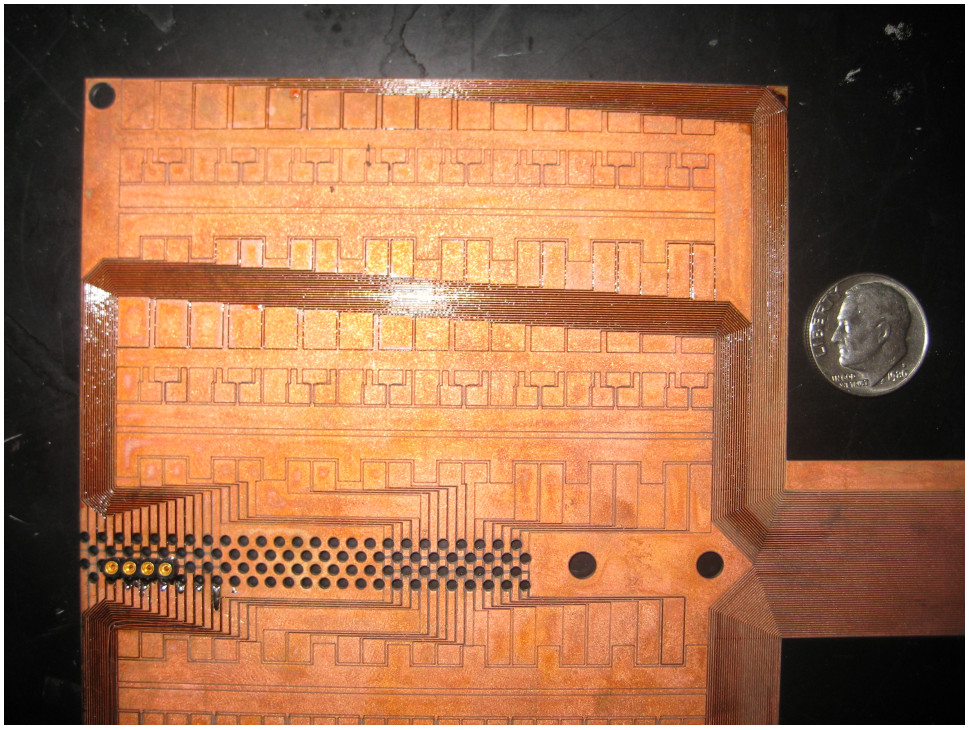

Figure 3.3: A previous design with an area ≈ 160 cm^2. Several problems with this design inspired the modular design described in this thesis.

In order to make the chips modular, the large leads had to be distributed on both sides of the chip. By distributing the leads on both sides of the slowing region, the consumed area was kept to a minimum. A series of these chips can be stacked with their slowing regions parallel to create any desired slowing length. Fig. 3.4 shows five chips combined together to create the final 60 wire slowing chip.

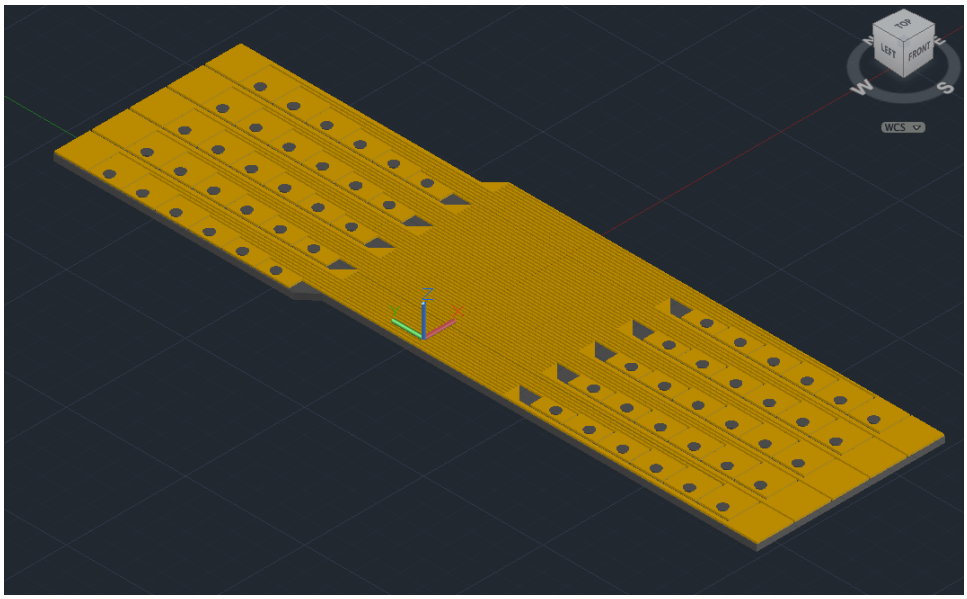

Figure 3.4: Five modular slowing chips combined to make a 60 wire slowing chip.

Unfortunately, while the modular design simplifies the chip fabrication, it increases the complexity of the chip control structure. Each wire must be controlled by a transistor. We desire to use the same transistor channel type, as P-channel transistors have different operating characteristics as N-channel transistors. Using the same channel type means that, for all transistors in our system, we must make a choice. Either all currents enter the drain pin and exit the source pin of the transistor (N-type), or vice-versa (P-type). Meanwhile, we operate with the constraint that the current in each wire must flow in the same direction across the slowing chip to allow the Lorentzian potential to transfer from wire to wire.

Imagine the current flows left to right across the chip. For the leftmost leads, the current would flow from a voltage, through a drain pin, out the source, up to an individual lead, across the chip to a common bus connected to ground.

However, for the rightmost leads, current must flow from a voltage on the leftmost bus, across the chip to an individual lead, through a drain pin, out of the source pin which is connected to ground.

Notice that for the leftmost leads, only the source pins need be independent. The drain pins may be joined to a common voltage. The opposite is true for the rightmost leads. The drain pins must be independent, while the source pins may be joined to a common ground. This idea is drawn schematically in Fig. 3.5.

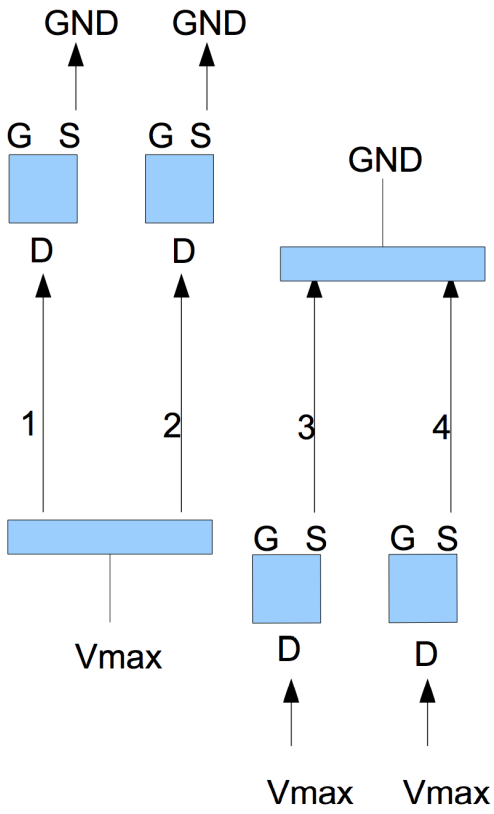

Figure 3.5: The placement of the transistors with respect to the slowing wires such that all currents flow in the same direction.

While we are using only N-type transistors, we can nevertheless identify two types of transistors for our circuit: those with tied drains and those with tied sources. The modular design will force us to use six tied drains, then six tied sources, then six more tied drains, etc. We will have to build a control structure to accommodate this layering in later sections.

3.2.2 G-Code and Laser Cutting.

Once the chip was drawn in AutoCAD, the 2D drawing was saved as a .dxf file and converted into a .pgm file which could be read by the laser cutting machine. The .pgm file contained simple G-Code instructions for a CNC mill. The laser output was pulsed at a 2000 kHz frequency. Each pulse, the laser would blast away a chunk of material. Then, the laser would move, and a pulse would be delivered to a new location. Thus, the laser made multiple passes over the same shape to achieve a continuous cut. The depth of cut was determined by how many times the laser passed over the same region.

A double-sided DBC/AlN was prepared by first cleaning the DBC surface with steel wool, acetone, and methanol. After the cleaning, a fresh sheet of printer toner was printed onto toner paper. The toner paper was folded around the chip and run through a laminator. The laminator's heat transferred the toner to the chip. By splashing water on the chip and paper, the paper could be removed, and the toner covered chip retrieved. The chip was then folded between a sheet of acid resist, and pushed through the laminator again. The resist bonded to the toner, providing an acid resisting layer for the upcoming etching process.

The prepared chip was then marked and centered on the laser cutting machine. The laser was focused to the same height as the DBC/AlN. The laser power was controlled by setting the diode current. After compiling the G-Code instructions, the laser began cutting the chip.

3.2.3 Acid Etching.

After the chips were cut, they were flipped over, and the copper around the through holes on the backside was laser cut away. The finished chips were then acid etched in a solution of hydrogen peroxide and hydrochloric acid. This removed any excess copper from between the traces. After testing the electric isolation of the traces using a voltmeter, the acid resist layer was removed with acetone.

3.2.4 Constructing the Chip.

Five modular chips were then vacuum epoxied together. A joining wire was soldered to each row of busses. As a result of a prior failed attempt, we had a broken chip, which was epoxied as a strengthening splint to the good chip. Then, 60 22 AWG wires were placed through the holes in the chips, and soldered to their corresponding leads. The "slowing chip" is shown in Fig. 3.6.

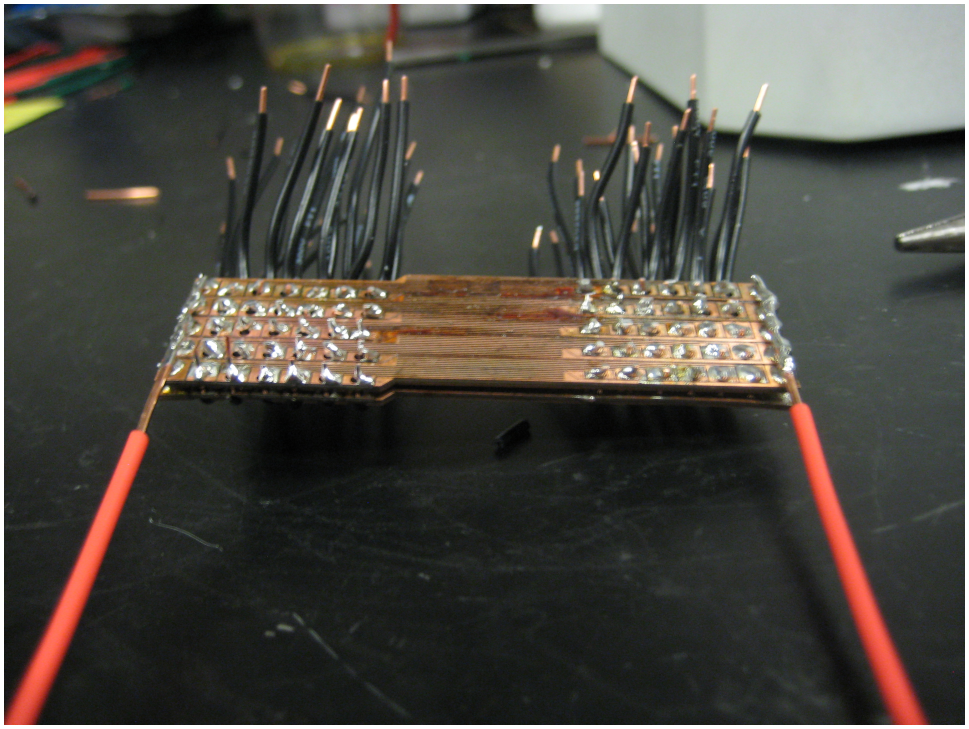

Figure 3.6: The slowing chip with all 60 leads soldered into place.

3.3 Making the Control Boards

3.3.1 Transistors.

The 60 wires from the slowing chip were soldered to a motherboard of 60 transistors, lined up in two rows of 30 on a 0.1 inch grid perforated prototyping board of plated through holes. On one row, the drains were soldered together, and the sources ran up to the left side

of the chip. For the other row, the source pins were soldered together, and the drains independently connected to the slowing chip. This arrangement allows all the transistors to be standard N-channel MOSFETs, as discussed above.

3.3.2 Breakout Board.

The transistor gates from the motherboard were transferred down to a breakout board for a 100 pin D-Subminiature connector. The gate wires were soldered into place corresponding to the 64 digital input/output pins from the Viewpoint Systems Digital Input/Output System. The transistor motherboard and the 100 pin breakout board are shown in Fig. 3.7.

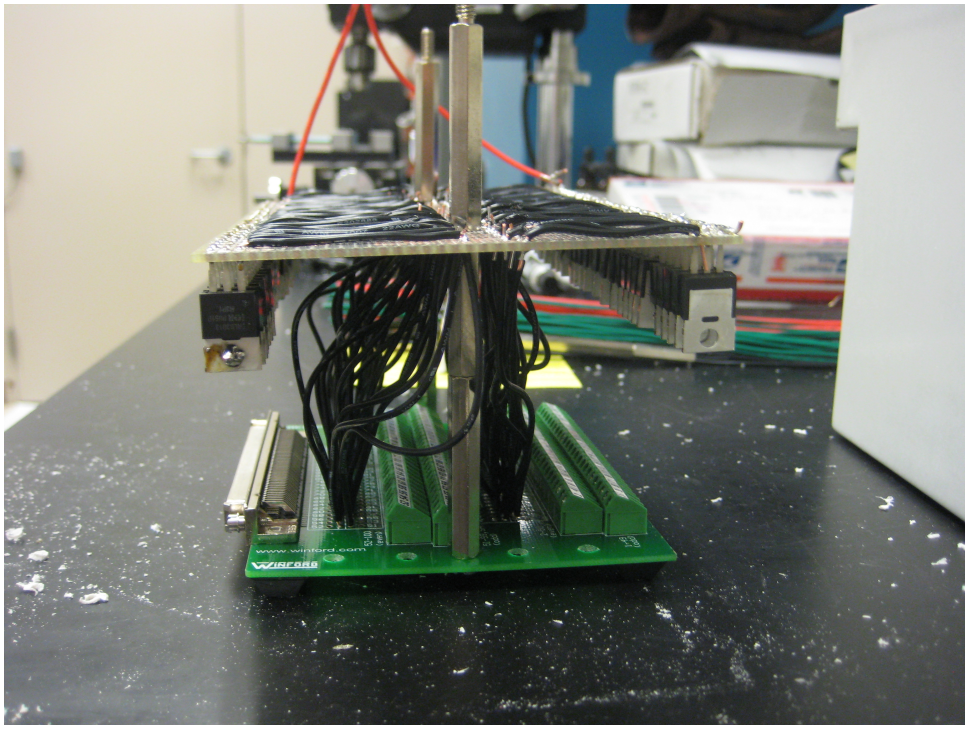

Figure 3.7: The transistor motherboard and the 100 pin breakout board.

3.3.3 Finishing the Chip.

An aluminum backing was cut to shape, and 60 18 AWG holes were precisely drilled to match the chip's through hole locations. Wires were epoxied into these holes using J.B. Weld. The wires were then stripped and soldered to the leads from the chip. The final structure, including the upper slowing chip, the aluminum backing, the transistor motherboard, and the 100 pin breakout board, was mounted into a hard plastic enclosure, and shown in Fig. 3.8.

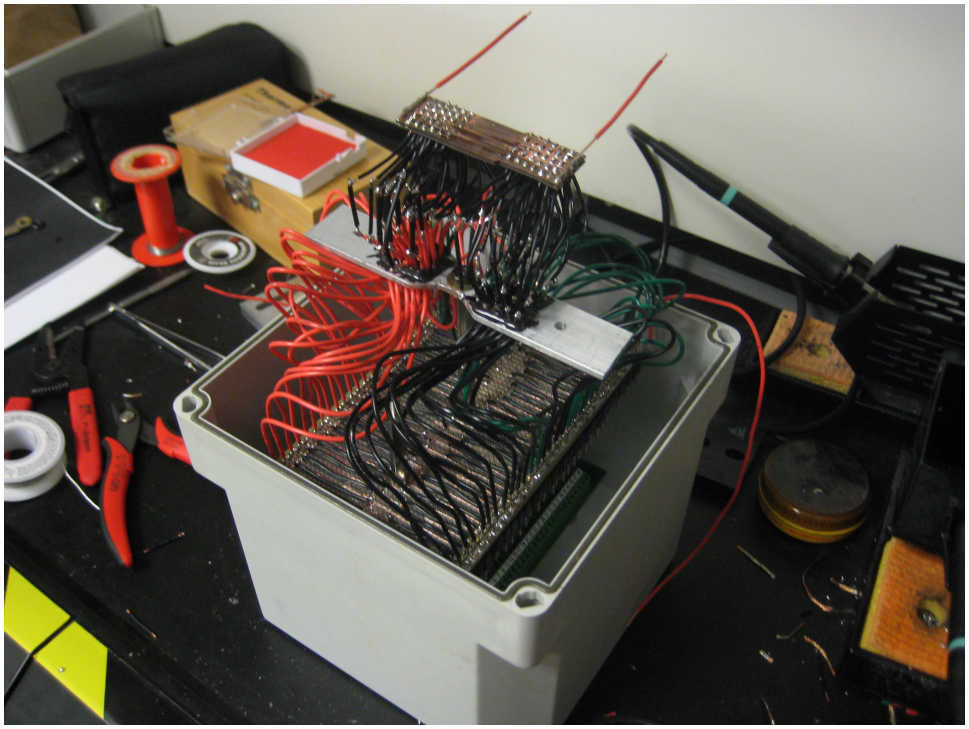

Figure 3.8: The full structure of the slowing chip.

3.4 Making the Chambers

3.4.1 MOT Chamber.

The $2D^+$-MOT chamber uses anti-reflection coated glass specific to the MOT laser frequency. The glass was cut and ground to create 5 pieces: 2 similar sides, 2 similar top

and bottom pieces, and one end cap. After using vacuum grade epoxy to construct a 5-sided, open-ended chamber, a separate DBC/AlN chip with a central hole was etched to provide the final sealing cap.

After the etch, two copper leads were pried from the AlN surface and crimped together with a capsule of Rubidium Chromate. When current is passed between the leads, Rubidium is released into the chamber. Beneath the capsule, a square mirror with a central hole was epoxied to the center of the chip. Then the chip/mirror structure was vacuum epoxied to the open-ended glass cell to seal the chamber. Fig. 3.9 shows the $2D^{+}$-MOT chamber before and after sealing.

3.4.2 Slowing Chamber.

A slide of glass was cut to the same size as the slowing region on the slowing chip. Two NdFeO permanent magnets were aligned and epoxied $1/16^{th}$ of an inch apart. The two magnets were then epoxied onto the slowing chip. The magnets were exactly one inch long, while the chip was not as long. A thin glass spacer was ground and epoxied to the underside of the slowing magnets where they protruded over the edge of the slowing chip. The slowing chamber was now sealed in the transverse directions, with two smooth faces to in the longitudinal direction.

3.4.3 Observation Chamber.

Finally, an open-faced glass cell was drilled with a small hole. The open end of the cell was epoxied to a transition cell, which was mounted to an ion pump. The small hole was epoxied to the open side of the slowing chamber.

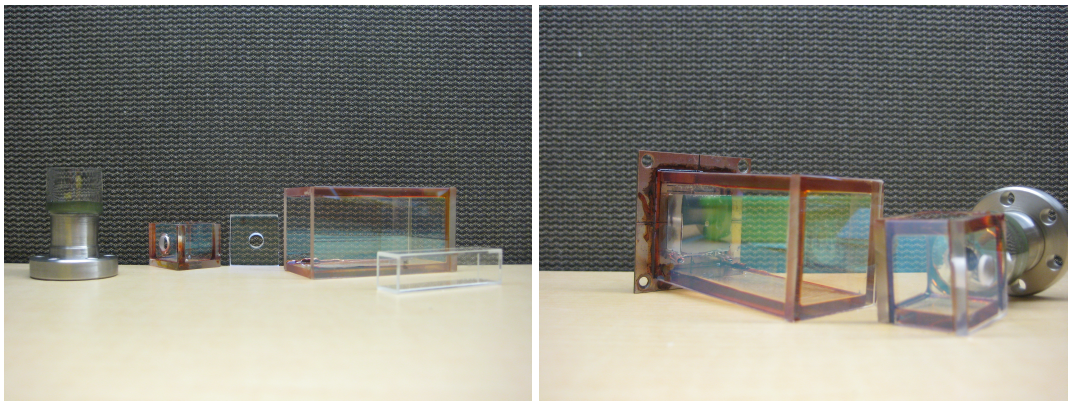

Figure 3.9: Left: (from left to right) the metal-glass transition cell, the observation chamber transition cell, the unfinished $2D^+$-MOT chamber, and the observation chamber. Right: (from left to right) the finished $2D^+$-MOT chamber and the finished combined transition cell.

3.5 Assembling the Apparatus

3.5.1 Combining the Pieces.

With each chamber completed, it was time to join them into a sealed system. The most fragile connection was also the first. The comparatively heavy $2D^+$-MOT chamber needed to be vacuum epoxied to the unsupportable and fragile slowing chip.

First, the slowing chip and its supporting structure were removed from their hard enclosure and mounted to a breadboard. Using holes in the DBC/AlN sealing chip, mirror rods were used to connect the $2D^+$-MOT chamber to a 3D-mount. A perpendicular breadboard was mounted to the original, and the mount was bolted to the perpendicular board.

When the breadboards were rotated, the 3D-mount could now act as a lowering crane, gently allowing the surfaces of the two chambers to come into contact. This delicate joining is shown in Fig. 3.10.

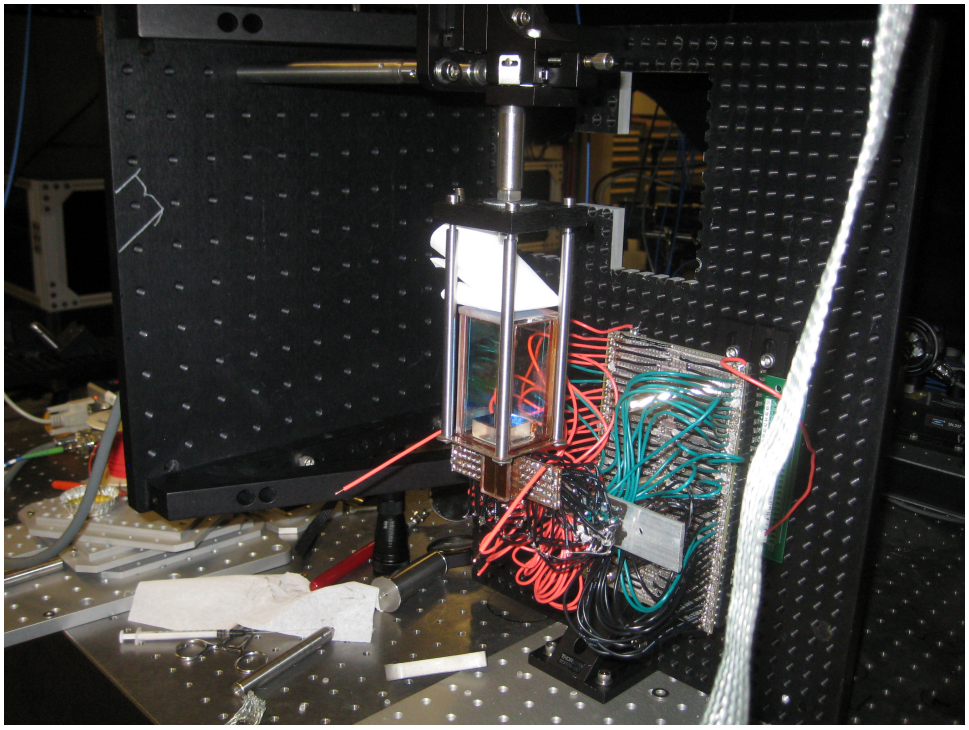

Figure 3.10: The joining of the 2D$^+$-MOT chamber with the slowing chamber.

Once the surfaces came into contact, they had to be epoxied together. The epoxy must be cured at high temperatures. However, as it cures, the epoxy becomes runny and viscous, flowing via capillary action into crevices. We were very concerned with semi-cured epoxy running into and sealing the bore between the two chambers. Great care was taken, and epoxy was applied using syringes with fine, thin, flexible tips. Even so, epoxy had to be continuously wicked away during the heating process. Eventually, the connection was made with the bore clear. The heavy 2D$^+$-MOT chamber was supported with a post and the system was brought back to its horizontal position.

The process was repeated to join the observation chamber to the opposite side of the slowing chamber, as shown in Fig. 3.11. The observation chamber was much easier to attach as the connecting hole was significantly larger than the bore. The wider surface allowed us to be more confident that we would not seal the bore.

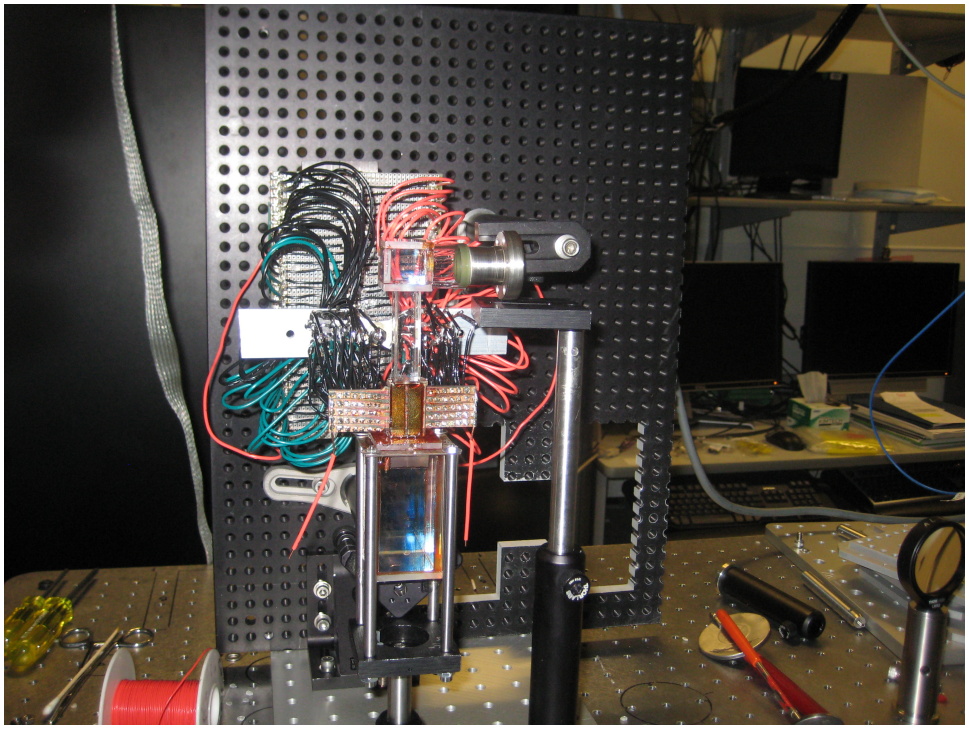

Figure 3.11: The joining of the observation chamber with the slowing chamber (top-down view).

3.5.2 Connecting the Pumping System.

The ion pump was connected to a nude ion gauge for pressure readings, and then connected to a removable system including a turbo pump and residual gas analyzer (RGA). These connections were made by screwing together two CONFLAT, knife-edge seals with a copper gasket in between. However, when the final connection was to be made, from the glass transition chamber to the metal pumping system, significant torque was required to screw the connection closed. This torque was high enough to snap the epoxied $2D^{+}$-MOT chamber from the slowing chamber.

While the break did not damage the chip, it forced an awkward repair process. The spacer glass which had previously been epoxied to the underside of the magnets had broken

and remained epoxied to the face of the 2D$^+$-MOT. It was impossible to remove the glass, meaning a connecting structure had to be built to rejoin the slowing and MOT chambers.

Using AutoCAD, several designs were tried to fix the problem. Eventually, a six-piece solution was found, shown in Fig. 3.12. A new spacer glass (shown in yellow) would be ground and epoxied to the old spacer (now the surface of the MOT chamber) on one side, and under the magnets to the slowing chip on the other side. Then, two channel separating slides (shown in brown) would be ground the same 1/16" height as the slowing magnets, and epoxied on either side of the bore, flush against the MOT chamber surface. A piece of glass (green) would be placed above these channel separators, flush to the MOT chamber surface. Another piece of glass (pink) would mate to the previous glass to provide a top seal. Finally, two (red, only one shown) pieces of glass would seal the sides of the new connection. The final repair is shown in Fig. 3.13.

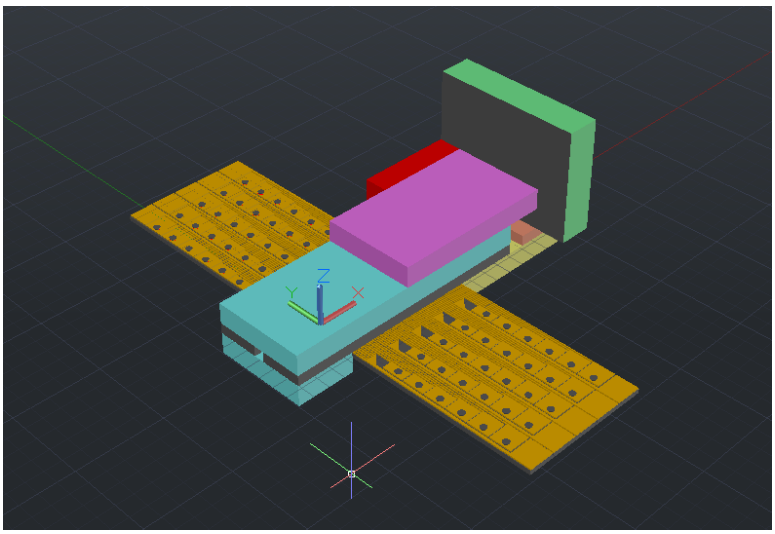

Figure 3.12: A drawing used to plan the rejoining of the 2D$^+$-MOT to slowing chamber. The new lower spacer is shown in yellow, the channel separating glass (only one is visible) is shown in brown, the top-sealing glass pieces are shown in green and purple, and the side-sealing glass (only one shown) is seen in red.

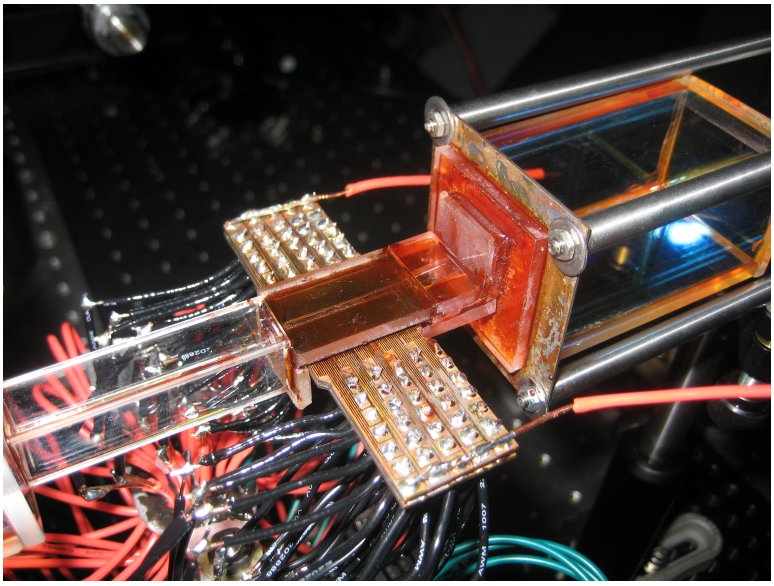

Figure 3.13: From left to right, the observation chamber, the slowing chamber, with its corresponding confining magnets and slowing chip, the repaired $2D^+$-MOT to slowing chamber connection, and the $2D^+$-MOT chamber. The wiring for the transistor support structure recedes into the background.

3.5.3 Baking Out the System.

Once the pumping system was in place, the turbo pump was turned on. Initially, there were several vacuum leaks. The largest were discovered by spraying methanol onto the chambers and watching where it entered the chambers. These leaks were sealed with more vacuum epoxy. After these larger leaks were sealed, the pressure reached $\approx 10^{-3}$ Torr. To identify the remaining leaks, compressed helium was gently blown towards specific parts of the chambers, while the RGA identified any partial pressure spikes corresponding to helium. These smaller leaks were sealed using VacSeal. After the smaller leaks were sealed, the pressure reached $\approx 10^{-7}$ Torr.

The system was then prepared for baking. Heating tape and aluminum foil were wrapped around the metal pumping system, whose temperature was monitored by an

inserted thermocouple. Aluminum foil was folded over the chip and a fan blown underneath to prevent overheating. Then two hot air guns were used to heat the glass chambers. The overall setup is shown in Fig. 3.14. After the bakeout, the pressure reached $\approx 10^{-8}$ Torr.

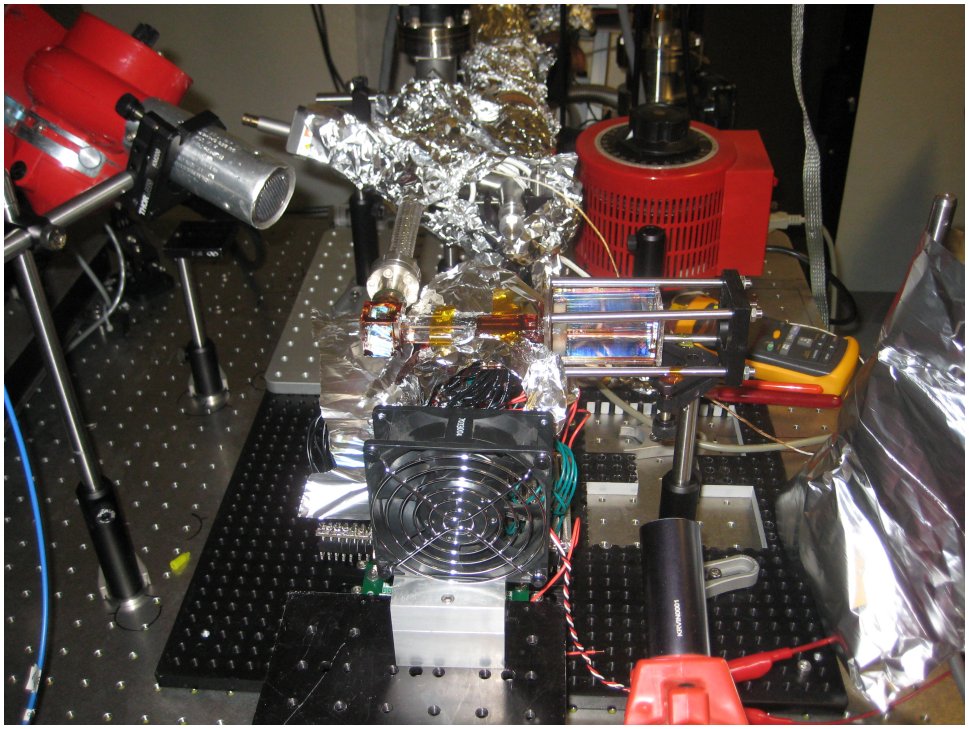

Figure 3.14: The experiment during the bakeout stage of vacuum pumping.

3.5.4 Preparing the MOT Chamber.

Creating a MOT requires a very low pressure in the $2D^+$-MOT chamber ($\approx 10^{-7}$ Torr). Because of the small slowing chamber connecting the $2D^+$-MOT chamber to the rest of the system, the pressure in the $2D^+$-MOT chamber was likely significantly higher than the reading from the nude ion gauge. We therefore pumped the system until the nude ion gauge read $\approx 10^{-8}$ Torr.

We then ran current through the rubidium chromate capsule. Initially, the capsule had absorbed a wide array of impurities from the atmosphere. The current was run at 5 A to

burn out and release these impurities. Once the impurities had been released, the capsule filled the chamber with rubidium. The rubidium acted as a getter material, further removing impurities. After these efforts, the vacuum system registered its lowest nude gauge reading, 3.3 X 10^{-9} Torr.

3.5.5 Creating the MOT.

We then began to construct the MOT itself, whose setup (viewed along the axis of the atom beam) is depicted in Fig. 3.15. Four permanent NdFeO magnets were epoxied to mirror rods and moved into position via a 3D translation mount and a mirror mount. These magnets create a magnetic field zero at their center.

The $2D^+$-MOT requires two equal power laser beams to intersect and reflect back on themselves in the transverse directions to the atomic beam. These "cooling" lasers are slightly detuned from the $5S_{1/2}(F = 2) \rightarrow 5P_{3/2}(F = 3)$ transition of ^{87}Rb [2]. The laser approaching from opposite the direction of the field requires σ^+ circularly polarized light, while the other requires σ^-. By detuning the lasers, only atoms traveling towards a given beam will absorb photons, and thus receive a momentum kick back towards the laser intersection.

Meanwhile, it is possible that an atom will transition into a "dark state" that no longer absorbs the cooling frequency. Thus, a second, lower intensity laser frequency is superimposed on the cooling light. This "repump" laser excites the atom back into a state where it can absorb the cooling frequency.

But this "optical molasses" only slows the atoms in the direction of the beam. The four magnets create the magnetic trap which allows the slowed atoms to congregate at the trap minimum. These atoms have been slowed in the two directions of the intersecting cooling beams, and thus form a beam in the third direction.

An optional third laser beam, called a "push beam," can be directed in the atomic beam direction. The push beam can make the beam's forward propagation slower, and was the

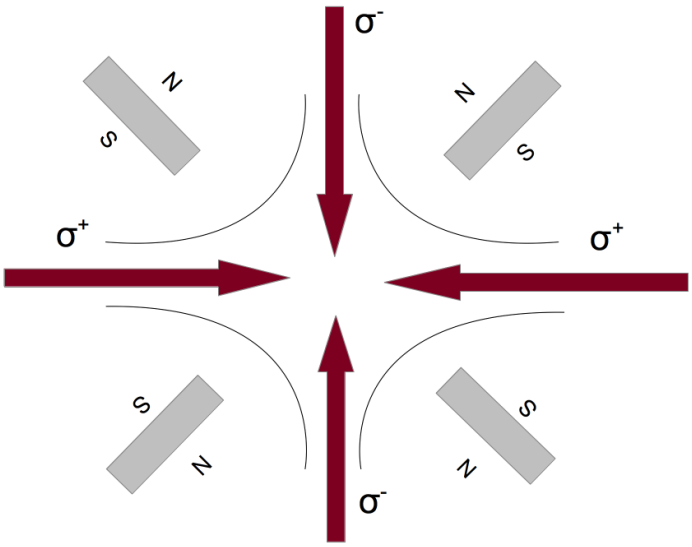

Figure 3.15: The MOT configuration using four permanent magnets and two intersecting, retroreflecting laser beams.

reason we inserted a mirror with a hole at the center on the atom beam axis in the $2D^+$-MOT chamber.

Laser light was split into two optical fibers, and then each was passed through two perpendicular cylindrical lenses to create an elliptical beam profile. Two mirrors reflected the beams directly back on themselves.

3.5.6 Aligning and Detecting the Atoms.

The four magnets in the $2D^+$-MOT configuration form a magnetic minimum where the atom beam is created. The beam must then be directed through the hole in the $2D^+$-MOT chamber, through the slowing chamber, and into the observation chamber on the opposite side. There, the atoms can be observed by the difference measurement of the probe laser discussed above.

The magnetic minimum, and thus the beam position and approach angle, can be manipulated by moving the magnets of the $2D^+$-MOT. Using the 3D and mirror mounts attached to the magnets, a great deal of time and effort was spent trying to align the beam to travel through the bore of the chamber without hitting any walls.

The alignment was achieved, and atoms were observed in the difference measurement of the probe laser. Once the beam was aligned, a second magnet was brought near the chamber, shifting the position of the beam. A corresponding dip in on the scope was registered. At this point, we were still setting up and troubleshooting the system, so no data was taken.

To make sure this dip was not caused by scattered light from the new magnet's surface, the repump laser was pulsed on and off. The majority of scattered light comes from the cooling light, not the repump. When pulsed, the beam appeared and disappeared, registering dips on the scope each time.

However, when the second magnet was brought in to misalign the $2D^+$-MOT by misaligning its magnetic field, the pulsed repump light showed no effect on the scope.

While no measurements were recorded at this point, we are confident atoms were guided through the slowing chamber.

3.5.7 The Complete System.

The completed system is shown in Fig. 3.16. The central slowing chip and its supporting structure are prominent in the middle, while the steel pumping apparatus recedes into the background. The large lens on the far left is an infrared camera looking down the bore of the slowing chamber. The blue optical fibers carrying the cooling and probe light snake throughout the system, while the two red leads provide current to the $2D^+$-MOT capsule of Rubidium Chromate. The remaining structure on the right side of the system are the lenses, mirrors, and magnets required to make the $2D^+$-MOT atomic beam.

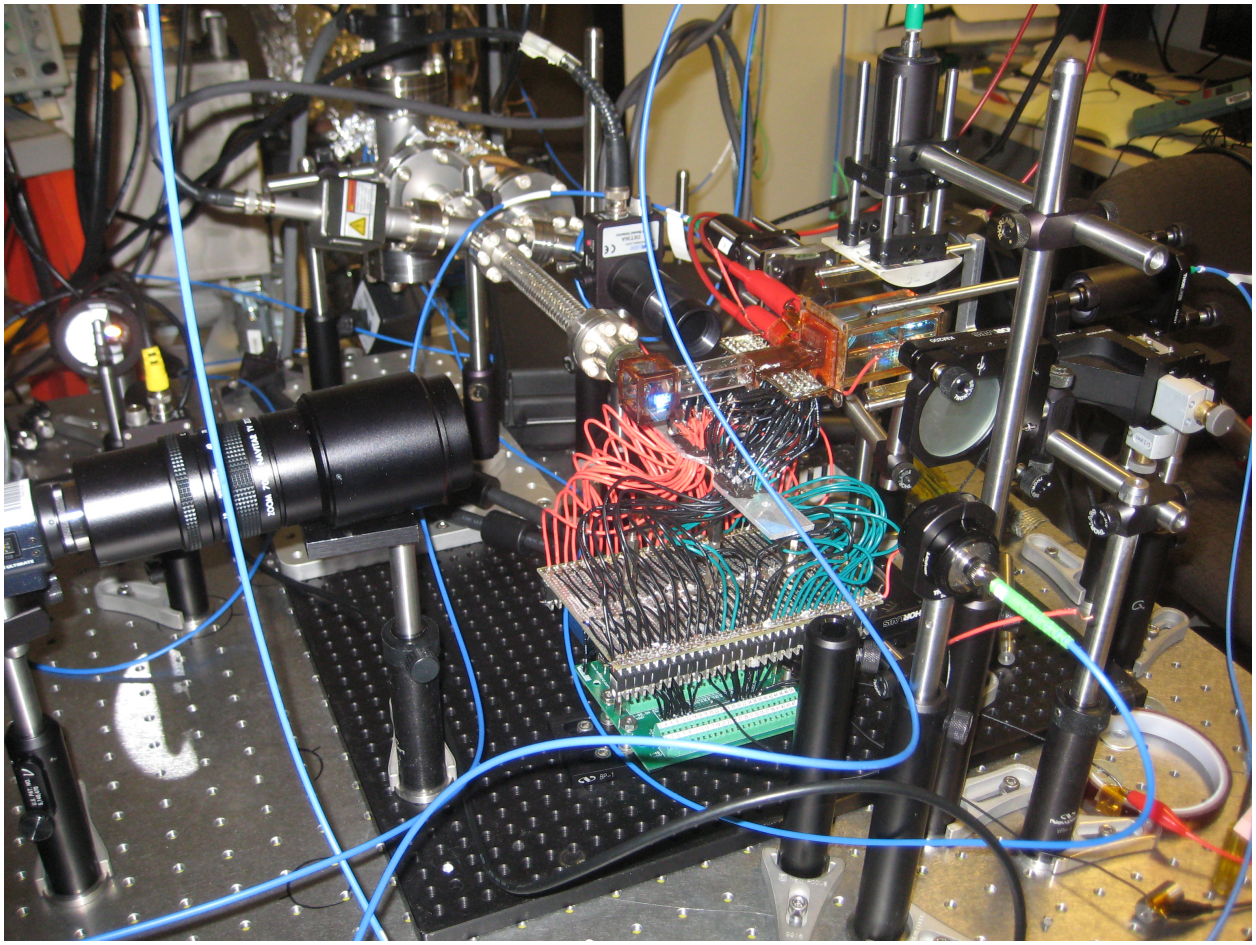

Figure 3.16: The completed system.

IV. Experiment and Results

4.1 Determining Operating Values

Current running through a wire on the slowing chip will create a maximum potential energy

$$V_{max} = \frac{m_F g_F \mu_0 \mu_B I}{2\pi\alpha} \tag{4.1}$$

which we want to be greater than the synchronous particle's total energy, which is $E = mv_0^2/2$. Thus, the required current is

$$I = \frac{\pi\alpha m v_0^2}{m_F g_F \mu_0 \mu_B} \tag{4.2}$$

We will be using ^{87}Rb in the $m_F = 2$ state withe g_F=1/2. For the 2D$^+$-MOT, $v_0 = 8$ m/s, and $\alpha = 800$ μm. With these values, the required current will be $I = 1993$ A, an absurdly high value for practical purposes. However, by decelerating the magnetic potential from a starting velocity matching that of the synchronous atom, our three dimensional model showed we could capture most of the beam pulse with just 200 A currents.

Because matching the velocity of the synchronous atom is so critical to this experiment, it is imperative that the currents can switch between wires in a short enough time interval. The atom is initially moving 8 m/s, and the spacing between wires is 330 μm, so the currents must switch within $2\beta/v_0 = 41.25$ μs.

Before running the experiment, we needed to find what parameters would achieve these operating values.

4.2 Achieving Operating Values

The transistor turn-on time, the resistance of the circuit, and the current actually flowing through the slowing chip wires were vital parameters to running the experiment.

Oxidation, heating cycles, varying-quality solder joints, and several other factors had modified the performance we expected from the performance detailed in each component's data sheet.

We created two twelve wire test chips and connected them to a motherboard of transistors using similar lengths and gauges of wires to the actual experiment. The test circuit is shown in Fig. 4.1. A digital power supply connected through a transistor to the test chip. The transistor's gate was controlled by a signal generator, providing a voltage between the gate pin and ground after the chip's resistance. The signal generator was set to give a square pulse voltage. The internal capacitance of the signal generator created an exponential turn on with a characteristic $1/e$ time $\approx$ 20 μs. On those short time scales, the signal generator would overshoot from the intended value and oscillate as it searched for the correct voltage. An example of the signal generator's voltage output is shown in Fig. 4.2. Finally, a four-lead voltage measurement was made across the chip. Knowing the output current from the power supply, this voltage drop gave the chip resistance according to Ohm's law.

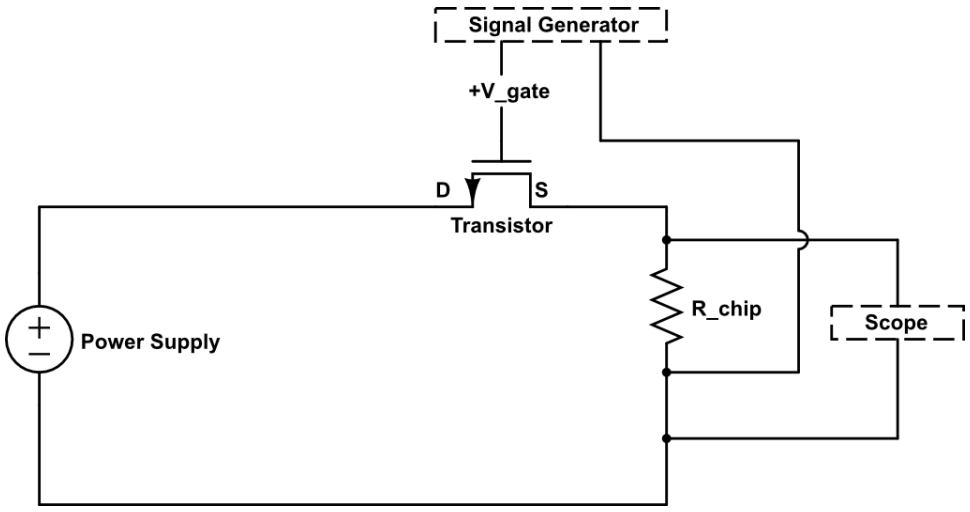

Figure 4.1: The test chip circuit.

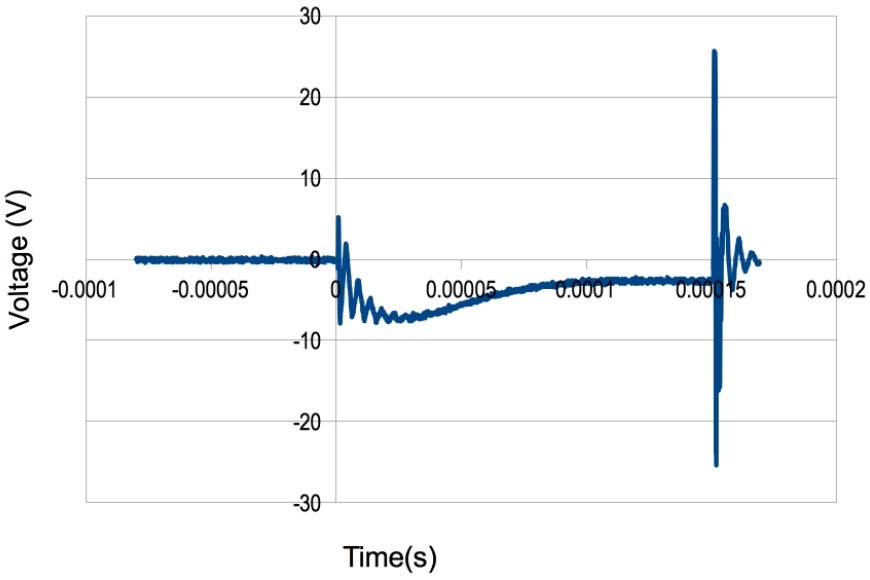

Figure 4.2: The output from the signal generator on short time scales.

We calibrated the chips at low currents from the power supply to understand the resistance of chip slowing wire. However, the power supply could not provide the 200 A currents we desired. After calibration, the power supply was replaced with an industrial-

scale capacitor charged to a known voltage. Then, using this voltage and the calibrated resistance, the current flowing across the chip was calculated.

The oscilloscope was capable of reading ultra-fast signals. However, scopes have unreliable grounds, and thus are not suitable for precise measurement of voltage. Precision can be attained using a digital multimeter (DMM), but those available in the lab did not have the capability to temporally resolve signals < 100 ms.

In order to have a valid concept of the current flowing in short time intervals, we calibrated the oscilloscope using a digital multimeter at low currents and long time intervals. Then, assuming the calibration remained valid at high currents, we could use the scope to determine current.

4.2.1 Test Chip 1.

The first test chip's calibration is shown in Table 4.1. As current increases, the scope voltage and DMM voltage increase at the same rate. The maximum current the power supply could output was 5 A, so we attribute the slight difference at that current to being on the extreme edge of the supply's operating range. We were therefore confident that the scope's voltage could be used reliably to ascertain current.

Table 4.1: 1 Hz Duty Cycle, 500 ms Pulses, 4 V Gate.

Current (A)	Scope (mV)	DMM (mV)	R_{chip}(mΩ)
1 A	448	42.5	42.5
2 A	900	85	42.5
5 A	2360	229	45.8

The power supply was switched to a capacitor and charged to various voltages. The transistor gate was controlled at a 1 Hz duty cycle, now with 10 ms, pulses. The gate was

given 4 V. The scope's voltage readings were taken, and current calculated, with results shown in Table 4.2.

Table 4.2: 1 Hz Duty Cycle, 10 ms Pulses, 4 V Gate.

Voltage (V)	Scope (V)	Current (A)
5 V	18.2	40.6
10 V	22.8	50.9
13.8 V	22.8	50.9

The added voltage from 10 V to 15 V did not change the current, implying the transistor's gate was limiting current flow. The gate voltage was taken to 10 V to ensure the transistor would turn completely on. Then, the 13.8 V capacitor gave a 121.4 A current. The current turned fully on in 50 μs.

While the signal generator was creating 10 V, there was a long length of wire connecting the ground back to the negative terminal of the capacitor. It is likely that this length of wire added a significant enough resistance to make the effective gate-source voltage less than was necessary to turn the transistor fully on. The extra length of wire was removed, and the experiment rerun under the same parameters. Now, the chip wire failed, likely because of the high current allowed to pass by the higher gate-source voltage.

4.2.2 Test Chip 2.

Once a new wire was connected, the gate-source voltage was brought back down to 4 V. The wire was recalibrated, with the results shown in Table 4.3.

Table 4.3: 1 Hz Duty Cycle, 500 ms Pulses, 4 V Gate.

Current (A)	Scope (mV)	DMM (mV)	R_{chip}(mΩ)
1 A	520	49	49
5 A	2880	271	54.2

The capacitor was charged to 12.5 V, and the gate-source voltage was tested at various levels. The pulses were shortened to 100 μs. The results are shown in Table 4.4.

Table 4.4: 1 Hz Duty Cycle, 100 μs Pulses.

G-S Voltage (V)	Scope (V)	Current (A)
3 V	25.2	48.4
4 V	50.4	96.9
5 V	62.4	120
6 V	62.4	120
10 V	62.4	120

The same scope readings for the various gate voltages implies that the current was now being limited by the capacitor voltage. Leaving the gate voltage at 10 V, the capacitor voltage was increased, with the results shown in Table 4.6.

Table 4.5: 1 Hz Duty Cycle, 100 μs Pulses, 10 V Gate.

Voltage (V)	Scope (V)	Current (A)
11 V	56.0	107.7
12 V	61.6	118.4
15 V	77.6	149.2
20.8 V	97.6	187
22.0 V	106	206

Finally, the gate was reduced to 4 V, and the capacitors charged to a combined 22 V. These parameters gave a scope reading of 105 V, or a 201.9 A current. The scope output for this 100 μs pulse is shown in Fig. 4.3. Note that the turn on time was $\approx$ 50 μs due to the signal generator's internal capacitance. This turn on time is insufficient for the first few wire transfers described by $\zeta(t)$. To achieve the necessary turn on time, we now moved to controlling the system with the DIO-64. Fig. 4.4 shows the voltage generated by the DIO-64. The turn on time is now a mere 20 μs, small enough for the initial wire switching.

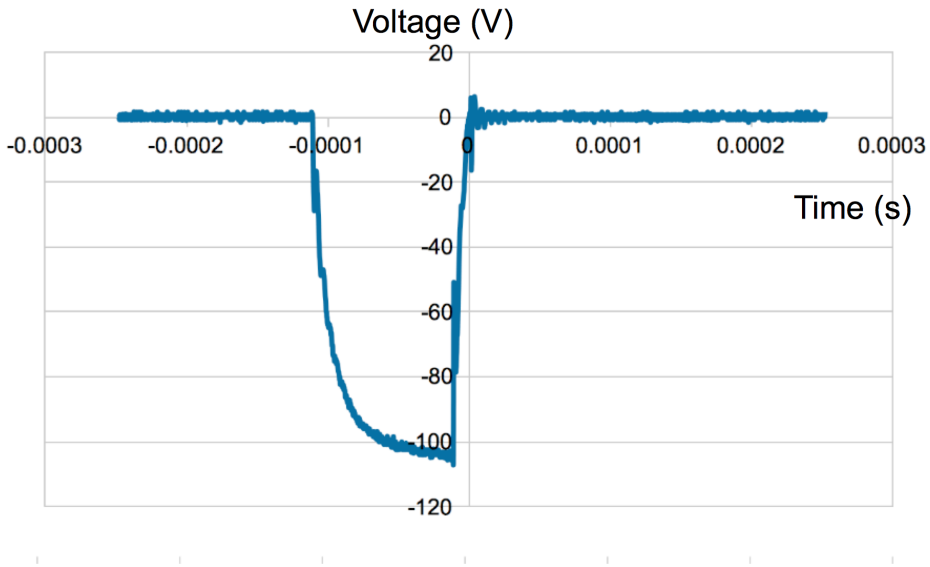

Figure 4.3: The scope output of the voltage drop as a function of time through the slowing wire. This profile corresponds to a maximum current of 201.9 A.

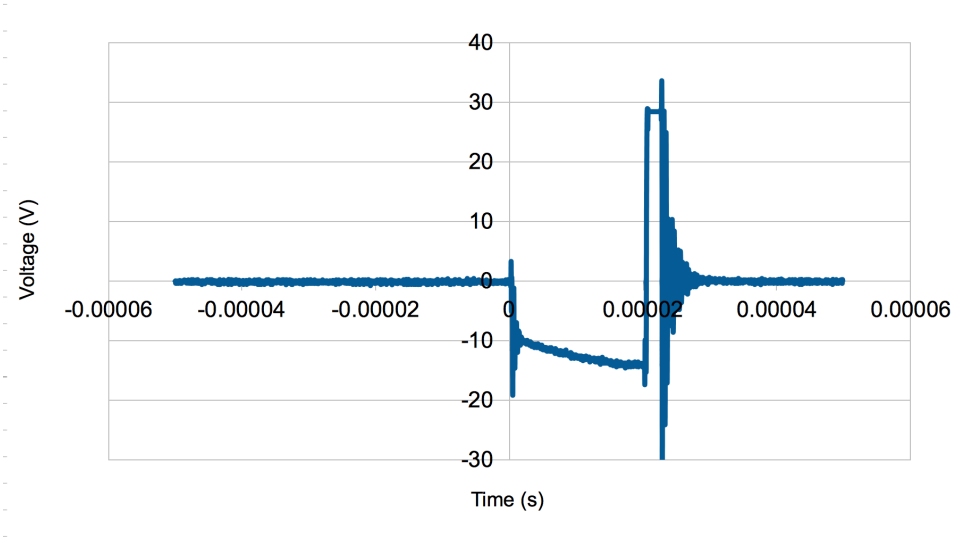

Figure 4.4: The faster voltage turn on time of the DIO-64.

These tests determined the parameters to create a 200 A slowing current. The capacitors would be charged to a combined 22 V while the gates would be digitally switched by the DIO-64 from Viewpoint systems from 0 to 4-5V. Thus, 200 A currents could be passed into the one desired wire at a given time within the switching times required by transfer function $\zeta(t)$.

4.3 Program to Control Currents

With the operating parameters determined, focus moved from the test chip to the actual slowing chip itself. The gate timing from the DIO-64 was controlled using an in-house developed program called Arbwave, by Spencer Olson. A python script was written to generate the length of each digital pulse corresponding to the exponential slowing described in previous sections.

The indexing of each wire was particularly difficult. Recall that each of the five combined chips carried six wires to a common bus left to right, and another six to a common bus right to left. Meanwhile, the motherboard carried two rows of 30 transistors. Additionally, current must flow in the same direction through the wires, regardless of which side has the transistor and which side has the bus. Thus, determining the sequence in which transistors should turn on was not straightforward.

The sequence and connections used for the chip are shown in Fig. 4.5. The "Line" values represent the sequential order in which the wires turn on. Line 1 turns on first, then Line 2, etc., until Line 60 is reached at the end of the slowing process. Each Line is next to a number. That number corresponds to a transistor on the motherboard, shown in two vertical columns like the physical arrangement. The numbered transistors then connect to the same number wire lead on the slowing chip, represented by the two 5 by 6 blocks in the center.

FET #	Order												Order	FET #
1	Line 49												Line 55	51
2	Line 50												Line 56	52
3	Line 51												Line 57	53
4	Line 52												Line 58	54
5	Line 53												Line 59	55
6	Line 54												Line 60	56
7	Line 37												Line 43	57
8	Line 38	6	5	4	3	2	1	51	52	53	54	55	56	Line 44	58
9	Line 39	12	11	10	9	8	7	57	58	59	60	61	62	Line 45	59
10	Line 40	36	35	16	15	14	13	63	64	65	66	85	86	Line 46	60
11	Line 41	42	41	40	39	38	37	87	88	89	90	91	92	Line 47	61
12	Line 42	48	47	46	45	44	43	93	94	95	96	97	98	Line 48	62
13	Line 25													Line 31	63
14	Line 26													Line 32	64
15	Line 27													Line 33	65
16	Line 28													Line 34	66
35	Line 29													Line 35	85
36	Line 30													Line 36	86
37	Line 13													Line 19	87
38	Line 14													Line 20	88
39	Line 15													Line 21	89
40	Line 16													Line 22	90
41	Line 17													Line 23	91
42	Line 18													Line 24	92
43	Line 1													Line 7	93
44	Line 2													Line 8	94
45	Line 3													Line 9	95
46	Line 4													Line 10	96
47	Line 5													Line 11	97
48	Line 6													Line 12	98

Figure 4.5: A schematic of the connections and their sequence within the gate control program.

4.4 Testing the Wires of the Actual Slowing Chip

After the wires could be independently turned on by Arbwave, each was individually tested at low current. Using low current and a circuit similar to Fig. 4.1, each wire was given a digital pulse to its transistor gate. The power supply's output current and the scope's voltage drop were recorded. The results are shown in Tables 4.6-4.8.

Table 4.6: Individual Wire Tests.

Line	Scope (V)	Current (A)
1	8.2	3.309
2	8.2	3.278
3	8.2	3.245
4	8.2	3.219
5	8.2	3.180
6	8.2	3.148
7	2.5	0.891
8	2.5	0.891
9	8.2	3.041
10	8.2	3.152
11	8.2	3.208
12	0	0
13	8.2	3.287
14	8.2	3.261
15	8.2	3.228
16	8.2	3.195
17	8.2	3.173
18	8.2	3.138
19	8.2	3.225
20	8.2	3.057

Table 4.7: Individual Wire Tests–Cont.

Line	Scope (V)	Current (A)
21	0	0
22	8.2	3.132
23	8.2	2.883
24	8.2	3.080
25	8.2	3.288
26	rapid oscillation between 0 and 8.2	2.12
27	8.2	3.231
28	8.2	3.198
29	8.2	3.150
30	8.2	3.118
31	8.2	3.225
32	8.2	3.193
33	8.2	3.167
34	8.0	2.8–
35	8.2	3.102
36	8.2	3.076
37	8.2	3.292
38	8.2	3.256
39	8.2	3.225
40	8.2	3.192

Table 4.8: Individual Wire Tests–Cont.

Line	Scope (V)	Current (A)
41	8.2	3.160
42	rapid oscillation between 0 and 8.2	2.02
43	8.2	3.245
44	8.2	3.195
45	8.2	3.165
46	8.2	3.135
47	8.2	3.098
48	8.2	3.076
49	8.2	3.278
50	8.2	3.244
51	8.2	3.208
52	8.2	3.174
53	8.2	3.143
54	8.2	3.115
55	8.2	3.237
56	8.2	3.185
57	8.2	3.155
58	0	0
59	8.2	3.090
60	8.2	3.066

In all, 52 out of the 60 slowing wires worked as expected, a significant achievement given the system's complexity. Two of the failed wires, lines 7 and 8, appear that their

failure is due to a simple electrical connection between them. The current ranges from 3.0 to 3.3 A, a 10% variation. The magnetic field of each wire varies proportionally to its current, so nearly 90% of our wires should create the expected magnetic field within a 10% variation. We expect to achieve a noticeable slowing of an atomic beam given such controlled error.

4.5 Running at High Current

While the tests at low current showed the slowing wires were able to be controlled as expected, high current tests showed an unforeseen flaw in the design. Because there are six pads and a bus on each side of a twelve wire slowing chip, two slightly different circuits created. On one side, the current crosses the slowing chip before reaching the transistor. On the other side, the current crosses the transistor before the slowing chip. The two circuits are drawn in Fig. 4.6.

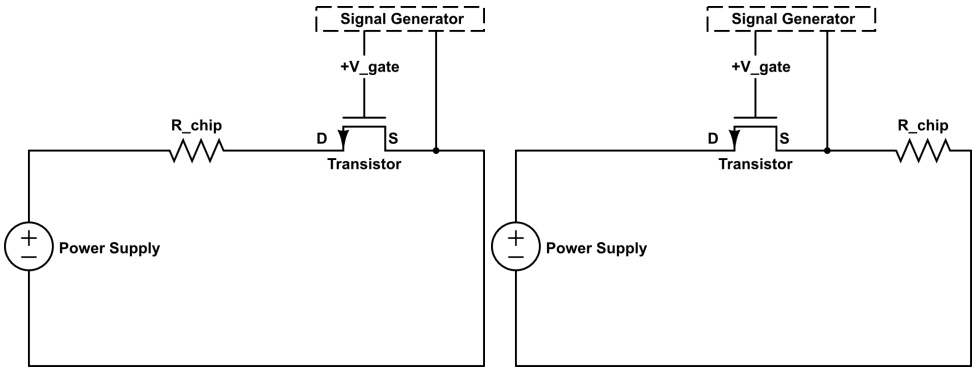

Figure 4.6: The two circuits depending on which side of the slowing chip the transistor sits.

On the side where the transistor comes after the slowing chip, the ground of the gate-source voltage connects directly to the negative pin of the power supply, ensuring the full voltage V_{gate} is seen by the transistor.

However, when the transistor comes before the slowing chip, the chip causes a voltage drop before reaching the negative terminal of the power supply. In other words, the transistor will not see the full voltage V_{gate}.

When we connected the power supply, any bad wires or open transistors should have been blown by the high current. That would leave only the isolated wires that had their transistors working to block current flow. After this purification step, we could independently control the remaining working wires through their gates.

We performed the purification step, and afterwards tested the wires at low and medium currents. At low current, the wires performed as expected, showing the transistors still functioned. However, as the voltage of the power supply was raised, current would continuously flow, as if a transistor had been left open with an unblown wire.

A continuously on transistor should have had its wire blown in the purification step, so we concluded that there must be a problem with the gate-source voltage. We tried several grounding techniques to address the problem, but none proved successful. In the end, each wire we tried to run at high current failed. The experiment remains intact with 50 remaining unblown wires while we try to identify the source of the problem.

V. Conclusion

Chip-scale magnetic cooling presents a unique set of challenges and a high degree of complexity to be overcome. The research done here has shown that, in theory, the benefit to be gained by continuous, time-dependent magnetic slowing is significant. Further, we have shown and built a full experiment which demonstrated several key aspects of the chip-scale atomic source.

- We have shown that the components required can be assembled into an ultra high vacuum system, capable of achieving pressures of 3.3 X 10^{-9} Torr.
- We have created a compact $2D^{+}$-MOT atomic beam source in short time, under the constraints of our design, and with minimal bakeout temperatures.
- We have achieved guiding of an atomic beam using permanent magnets through a $\approx 10^{-8}$ m^2 cross-sectional bore.
- We have detected the relatively low density $2D^{+}$-MOT beam as it emerged from guiding into the observation chamber.
- We have built and tested a slowing chip with 60 individually controlled, high current, 150 μm wires with an 90% success rate.
- We have built and tested a control system to achieve exponential magnetic slowing.
- We have identified difficulties and flaws to be corrected in subsequent designs.

While the experiment built here ultimately did not slow atoms, it represents a significant step towards that goal.

Ultimately, the transistor complexity caused the failure of the slowing chip at high current. The most immediate future work will be to reduce the number of transistors and

complexity of the overall control setup. A feasible option would be to design a modular chip with the transistors directly mounted. With the transistors surface mounted, much of the control system wiring could be removed. Another option is to embed a programmable microcontroller directly on the chip to replace the DIO-64. However, significant research must be done to find a microcontroller with fast enough switching times to transfer the magnetic potential.

Once the control structure is made more robust, there is work to be done characterizing the output beam. The present experiment could only detect beam slowing in the longitudinal direction by comparing the time-of-flight of the output atoms. It would be useful to characterize the beam dispersion, total density, and final velocities. One way to determine the velocity distribution would be to use a precise magnetic potential at the end of the slowing region which only allows a certain velocity or higher to pass. By measuring the observation laser absorption as a function of the blocking potential, a velocity distribution could be inferred.

If the chip-decelerator works as the above simulations suggest, there are essentially two different directions future research could take. First, the chip slower could be incorporated into a chip-based Bose-Einstein Condensate device, replacing the MOT as the initial source of cold thermal atoms. If successful, the achieved condensate would not rely on laser cooling, allowing an effort to create the first continuous-wave condensate.

On the other hand, the chip slower could be used to slow atoms and molecules previously thought too difficult. Research would progress to improve the density, collimation, and final velocity of the output beam to enable research and technology in cold chemistry, atomic clocks, and atom interferometry. With these parameters improved enough, the chip slower's compact design could underpin cold atom technologies outside the laboratory environment.

The numerous disruptive technologies enabled by cold atoms are being hampered by the insufficient modern methods of cooling. Chip-based magnetic deceleration promises a cooling mechanism to slow most neutral atoms and molecules within the cost and size requirements of a device in the field, whether that be Air, in the form of inertial navigation units, Space, in the form of GPS-enhancing atomic clocks, or Cyberspace, in the form of a quantum computer.

Appendix: 3D Modeling of the Slowing Chip

A.1 The Fields

The slowing chip can be modeled in three dimensions knowing the field due to current carrying wires in cartesian coordinates. For a $\hat{j}$ wire at position $(x, z) = (\alpha, \beta)$

$$\vec{B}_{\hat{j}} = \frac{\mu_0 I_j}{2\pi}\left[\left(\frac{(z-\beta)}{(x-\alpha)^2+(z-\beta)^2}\right)\hat{i} + \left(\frac{-(x-\alpha)}{(x-\alpha)^2+(z-\beta)^2}+\right)\hat{k}\right] \tag{A.1}$$

For a $\hat{k}$ wire at position $(x, y) = (a, b)$

$$\vec{B}_{\hat{k}} = \frac{\mu_0 I_k}{2\pi}\left[\left(\frac{-(y-b)}{(x-a)^2+(y-b)^2}\right)\hat{i} + \left(\frac{(x-a)}{(x-a)^2+(y-b)^2}\right)\hat{j}\right] \tag{A.2}$$

Our setup has a $\hat{k}$ beam. We require beam confinement, achieved either two oppositely magnetized permanent magnets. Because the magnetization is so large, we can assume movement in the transverse direction is small about the origin. Thus, we will model the confining field a quadrupole field from four wires in the $\pm\hat{k}$ direction. In the limit of small (x, y), the field is

$$\vec{B} = \frac{2\mu_0 I_{\hat{k}}}{d^2\pi}\left[x\hat{i} - y\hat{j}\right] \tag{A.3}$$

for the four $\hat{k}$ wires with positive $I_{\hat{k}}$ at locations $(\pm d, \pm d)$ and negative $I_{\hat{k}}$ at locations $(\pm d, \mp d)$. Let $d = \alpha$. We define two constants:

$$C = \frac{2\mu_0 I_{\hat{k}}}{\alpha^2\pi}\ ;\ D = \frac{\mu_0 I_j}{2\pi}$$

Then, if the $\hat{j}$ field moves according to $\zeta(t)$:

$$\vec{B}_{tot,x} = Cx + D\left(\frac{(z-\zeta(t))}{(x-\alpha)^2+(z-\zeta(t))^2}\right)\hat{i} \tag{A.4}$$

$$\vec{B}_{tot,y} = -Cy\hat{j} \tag{A.5}$$

$$\vec{B}_{tot,z} = D\left(\frac{-(x-\alpha)}{(x-\alpha)^2 + (z-\zeta(t))^2}\right)\hat{k} \tag{A.6}$$

Which gives a total field magnitude

$$|\vec{B}_{tot}| = \sqrt{\left(Cx + D\frac{(z-\zeta(t))}{(x-\alpha)^2 + (z-\zeta(t))^2}\right)^2 + C^2y^2 + D^2\frac{(x-\alpha)^2}{[(x-\alpha)^2 + (z-\zeta(t))^2]^2}} \tag{A.7}$$

which becomes

$$|\vec{B}_{tot}| = \sqrt{C^2(x^2+y^2) + 2CD\frac{x(z-\zeta(t))}{(x-\alpha)^2 + (z-\zeta(t))^2} + D^2\left(\frac{1}{[(x-\alpha)^2 + (z-\zeta(t))^2]}\right)} \tag{A.8}$$

A.2 The Forces

The potential energy is $V = m_F g_F \mu_B |\vec{B}|$. The forces on any given particle are given by $\vec{F} = -\nabla V$ evaluated at the position of the particle. So,

$$\vec{F}_x = m\ddot{x} = -m_F g_F \mu_B \frac{\partial}{\partial x}|\vec{B}_{tot}| \tag{A.9}$$

$$\vec{F}_y = m\ddot{y} = -m_F g_F \mu_B \frac{\partial}{\partial y}|\vec{B}_{tot}| \tag{A.10}$$

$$\vec{F}_z = m\ddot{z} = -m_F g_F \mu_B \frac{\partial}{\partial z}|\vec{B}_{tot}| \tag{A.11}$$

$$\vec{F}_x = \frac{-m_F g_F \mu_B}{2|\vec{B}_{tot}|}\left(2C^2x + D^2\frac{-2(x-\alpha)}{[(x-\alpha)^2 + (z-\zeta(t))^2]^2} + 2CD\frac{[(x-\alpha)^2 + (z-\zeta(t))^2](z-\zeta(t)) - 2x(z-\zeta(t))(x-}{[(x-\alpha)^2 + (z-\zeta(t))^2]^2}\right. \tag{A.12}$$

$$\vec{F}_y = \frac{-m_F g_F \mu_B}{|\vec{B}_{tot}|}C^2y \tag{A.13}$$

$$\vec{F}_z = \frac{-m_F g_F \mu_B}{2|\vec{B}_{tot}|}\left(D^2 \frac{-2(z-\zeta(t))}{[(x-\alpha)^2+(z-\zeta(t))^2]^2} + 2CD\frac{[(x-\alpha)^2+(z-\zeta(t))^2]x - 2x(z-\zeta(t))^2}{[(x-\alpha)^2+(z-\zeta(t))^2]^2}\right) \tag{A.14}$$

These forces can be integrated numerically to plot a particle's trajectory as a function of time through the Zeeman Decelerator described above.

Bibliography

[1] Hendrick L. Bethlem. Getting a handle on difficult atoms. *Physics*, 1(25):1–3, 2008.

[2] K. Dieckmann, R. J. C. Spreeuw, M. Weidemuller, and J.T.M. Walraven. Two-dimensional magneto-optical trap as a source of slow atoms. *Physical Review A*, 58(5):3891–3895, 1998.

[3] Daniel M. Farkas, Kai M. Hudek, Evan A. Salim, Stephen R. Segal, Matthew B. Squires, and Dana Z. Anderson. A compact, transportable, microchip-based system for high repetition rate production of boseeinstein condensates. *Applied Physics Letters*, 96, 2010.

[4] M. Holland, K. Burnett, C. Gardiner, J. I. Cirac, and P. Zoller. Theory of an atom laser. *Physical Review A*, 54(3), 1996.

[5] Samuel A. Meek, Horst Conrad, and Gerard Meijer. A stark decelerator on a chip. *New Journal of Physics*, 11, 2009.

[6] Sebastiaan Y.T. Van De Meerakker, Hedrick Behlem, and Gerard Meijer. Taming molecular beams. *Nature Physics*, 4:595–602, 2008.

[7] Edvardas Narevicius, Adam Libson, Christian G. Parthey, Isaac Chavez, Julia Narevicius, Uzi Even, and Mark G. Raizen. Stopping supersonic oxygen with a series of pulsed electromagnetic coils: A molecular coilgun. *Physical Reivew A*, 77(05140):1–4, 2008.

[8] Edvardas Narevicius and Mark G. Raizen. Toward cold chemistry with magnetically decelerated supersonic beams. *Chemical Reviews*, 112:4879–4889, 2012.

[9] Matthew Squires. Atomic physics for precision navigation and timing. *Presented to the Air Force Research Laboratory*, 2013.

[10] Matthew B. Squires, James A. Stickney, Evan J. Carlson, Paul M. Baker, Walter R. Buchwald, Sandra Wentzell, and Steven M. Miller. Atom chips on direct bonded copper substrates. *Review of Scientific Instruments*, 82(2), 2011.

[11] Epoxy Technology. Epo-tek 353nd technical data sheet. *Rev. XXVII*, 2012.

[12] A. Trimeche, M. N. Bera, J.-P. Cromieres, J. Robert, and N. Vanhaecke. Trapping of a supersonic beam in a traveling magnetic wave. *The European Physical Journal D*, 65:263–271, 2011.

REPORT DOCUMENTATION PAGE

Form Approved
OMB No. 0704–0188

1. REPORT DATE *(DD–MM–YYYY)*	2. REPORT TYPE	3. DATES COVERED *(From — To)*
13–06–2013	Master's Thesis	Oct 2011–Jun 2013

4. TITLE AND SUBTITLE

Chip-Scale Magnetic Source of Cold Atoms

5a. CONTRACT NUMBER

5b. GRANT NUMBER

5c. PROGRAM ELEMENT NUMBER

6. AUTHOR(S)

Imhof, Eric A., CTR

5d. PROJECT NUMBER

5e. TASK NUMBER

5f. WORK UNIT NUMBER

7. PERFORMING ORGANIZATION NAME(S) AND ADDRESS(ES)

Air Force Institute of Technology
Graduate School of Engineering and Management (AFIT/EN)
2950 Hobson Way
WPAFB, OH 45433-7765

8. PERFORMING ORGANIZATION REPORT NUMBER

AFIT-ENP-13-J-03

9. SPONSORING / MONITORING AGENCY NAME(S) AND ADDRESS(ES)

Dr. Matthew Squires
Cold Atom Group
Air Force Research Laboratory
Bldg. 1150, Kirtland AFB, NM

10. SPONSOR/MONITOR'S ACRONYM(S)

AFRL/RVBYE

11. SPONSOR/MONITOR'S REPORT NUMBER(S)

12. DISTRIBUTION / AVAILABILITY STATEMENT

DISTRIBUTION STATEMENT A:
APPROVED FOR PUBLIC RELEASE; DISTRIBUTION UNLIMITED

13. SUPPLEMENTARY NOTES

This work is declared a work of the U.S. Government and is not subject to copyright protection in the United States.

14. ABSTRACT

Numerous disruptive technologies are being hampered by the insufficient modern methods of cooling electrically neutral atoms and molecules. Microchip-based magnetic deceleration provides a cooling mechanism to slow most neutral atoms and molecules within the cost and size requirements of a real-world device. Simulations of a novel deceleration technique show 90% removal of kinetic energy from an atomic beam. An experiment is built which creates a time-dependent, decelerating magnetic field to slow an atomic beam. An atomic beam is magnetically guided 800 microns above the surface of a microchip at pressures of 10^{-9} Torr. A 60 independent wire microchip is fabricated, controlling 200 A currents through 150 micron wide wires with a 90% success rate. Flaws are identified and future efforts to correct them are discussed.

15. SUBJECT TERMS

Atomic Sources, Cold Atoms, Microchip Design, Bose-Einstein Condensate

16. SECURITY CLASSIFICATION OF:			17. LIMITATION OF ABSTRACT	18. NUMBER OF PAGES	19a. NAME OF RESPONSIBLE PERSON
a. REPORT	b. ABSTRACT	c. THIS PAGE			Dr. Glen P. Perram (ENP)
U	U	U	UU	82	19b. TELEPHONE NUMBER *(include area code)* glen.perram@afit.edu; 937-255-6565x4504